2019-01-01

HSPG2 Mediates Mandibular Jaw Joint Development

Barbara Samantha Castellanos
University of Texas at El Paso

HSPG2 MEDIATES MANDIBULAR JAW JOINT DEVELOPMENT

BARBARA SAMANTHA CASTELLANOS

Master's Program in Biological Sciences

APPROVED:

Anita M. Quintana, Ph.D., Chair

Chu Young Kim, Ph.D.

Jeffrey T. Olimpo, Ph.D.

Stephen L. Crites, Jr., Ph.D.
Dean of the Graduate School

HSPG2 MEDIATES MANDIBULAR JAW JOINT DEVELOPMENT

by

BARBARA SAMANTHA CASTELLANOS, B.S.

THESIS

Presented to the Faculty of the Graduate School of

The University of Texas at El Paso

in Partial Fulfillment

of the Requirements

for the Degree of

MASTER OF SCIENCE

Department of Biological Sciences

THE UNIVERSITY OF TEXAS AT EL PASO

December 2019

Acknowledgements

I would first like to acknowledge and thank my mentor, Dr. Anita Quintana, who took me on as a student in the last semester of my undergraduate career besides me knowing very little about working in a lab. I have learned various valuable lessons under your direction, and I feel that I have grown to be a more assured and thoughtful individual since working on my master's degree. I will forever be grateful to you for giving me all the help that you did.

I would additionally like to thank my committee members— Dr. Chu Young Kim and Dr. Jeffrey T. Olimpo, for all their time and valuable commentary. I extend my gracious thanks to my lab colleagues who were an invariable source of aid. You will all be valuable minds in the greater scientific community one day and I wish you all immense success.

Lastly, I would like to acknowledge my mother, who has stood beside and helped me even in situations where it was incredibly difficult for her to do so. I could spend an entire lifetime trying to pay you back for everything you have given me, and it would still never be enough. Thank you for all your love.

Abstract

We present a patient diagnosed with a multiple congenital anomaly syndrome characterized by scoliosis, intellectual disabilities, and craniofacial defects. Trio-based whole exome sequencing identified compound heterozygous variants in the *HSPG2* gene: a maternally inherited c.5998-7A>G variant in the promoter region and a paternally inherited c.4916C>T variant in the coding sequence. *HSPG2* encodes for perlecan, a large proteoglycan that plays an important role in cartilage formation, cell adhesion, and basement membrane stability. Mutations in *HSPG2* have been associated with Schwartz-Jampel syndrome and Dyssegmental Dysplasia Silverman-Handmaker Type, two disorders characterized by skeletal abnormalities (1). These data indicate a function for *HSPG2* in cartilage development/maintenance. However, the mechanisms by which *HSPG2* regulates cartilage development are not completely understood. To address this, we performed morpholino-mediated knockdown of *hspg2* in zebrafish. Knockdown of *hspg2* resulted in a 7% truncation in the mandible and a fusion of the mandibular jaw point at 5 days post fertilization (dpf). We surmised that defects in mandible development were a consequence of neural crest cell (NCC) function, as these multipotent progenitors produce the cartilage of the head and neck. Early NCC development was normal in morphant animals as measured by *dlx2a* and *sox10* expression at 1 dpf. However, subsequent analysis at later stages of development (3-4 dpf) revealed a decrease in the number of *sox10* and *col2a1a* positive cells within the mandibular jaw joint region of morphants relative to control injected embryos. Concurrently, morphants showed a decreased expression of *nkx3.2,* a jaw joint molecular marker at 2 dpf. Collectively, these data suggest a complex role for *hspg2* in jaw joint formation and late stage NCC differentiation.

Table of Contents

List of Tables

List of Figures

Chapter 1: Introduction

MULTIPLE CONGENITAL ANOMALIES

A multiple congenital anomaly (MCA) syndrome is characterized as two or more differently localized congenital defects in a single individual (2). The congenital defects present in these cases are classified as either major abnormalities (congenital heart defects) or minor abnormalities (a single palmar crease). While MCAs are generally rare (about 1-3% of newborns present with more than one major congenital anomaly at birth), infants with MCAs have longer hospital stays and increased mortality rates (3). Most congenital malformations observed in the first year of life (65-75 percent) are classified as having an "unknown" cause. However, even with such a large portion of congenital anomalies having seemingly unknown causes, these abnormalities collectively comprise over 15,500 of all recognized genetic disorders (4). While it is estimated that genetic mutations are the second largest cause of abnormalities (ranging anywhere from 15-25 percent), it is also likely that a significant proportion of malformations labeled as "unknown" are likely to have a genetic component as well. (4).

Recognized genetic causes are inherited mutations (which can either be autosomal or X-linked), *de novo* mutations (which appear in the individual without a hereditary context), chromosomal aberrations (which are abnormalities of chromosomal structure), and microinsertions or deletions (4). Although the interplay between genotype and phenotype is complex, genetic causes are still a major underlying cause of reported cases and therefore, it is vital to study the genetic etiology of patients diagnosed with MCAs. By studying the genetic etiology of patients, research can more readily uncover the mechanisms behind genetic factors causing disease (4).

PATIENT CASE

Central to our project is a patient case diagnosed with an MCA of unknown etiology. The patient presents with craniofacial abnormalities, idiopathic scoliosis, and an intellectual disability not found in either parent. To examine the patient case, whole exome sequencing (WES) of patient and related parents was sequenced.

WHOLE EXOME SEQUENCING AS A TOOL TO UNCOVER GENETIC ETIOLOGY

WES is a reliable scientific technique used to examine portions of the genome (5). This method sequences the exome (the portion of DNA which provides the backbone for creating functional proteins) because it is the genetic component most likely to give interpretable mutations that result in phenotypes (6). The mutations most reliably diagnosed by WES are missense and nonsense variants that are rare in the general population and have been previously reported as pathogenic, or insertion/deletions smaller than 50 base pairs within non-repetitive coding DNA (7).

WES is also a readily affordable technique. Initially, sequencing the genome was a lengthy and expensive endeavor, ranging anywhere from 20-25 million dollars per sample (8). Fortunately, WES emerged as a next-generation sequencing approach in 2008 and since then has functioned as a less expensive and rapid alternative to the original procedure (8). WES has most recently been used in patient cases presenting with craniofacial abnormalities, syndromic intellectual disabilities, and familial idiopathic scoliosis to identify variants in the *EFTUD2, SNRPA,* and *HSPG2* genes (9–11).

HSPG2 AND PERLECAN

HSPG2 (heparan sulfate proteoglycan 2) is a gene located on the human short arm *p* of chromosome one at position 36.12 (12). *HSPG2* encodes for a large, multidomain proteoglycan

known as perlecan, which, despite its size and general complexity, is well conserved across various vertebrate species (12). After intracellular modification, perlecan is secreted into the basement membrane, a region rich with glycoproteins, collagen, and laminins that separates the epithelium from underlying connective tissue. Perlecan is also found in cartilage, which makes up most of the skeleton during early development (12,13).

Perlecan consists of five domains. Domain I is unique to perlecan and plays an integral role in vertebrate tissue integrity and development. This domain consists of a module that shares homology with the Sperm, Enterokinase, and Agrin (SEA) domain of other extracellular matrix proteins, and glycosaminoglycan (typically a mixture of heparan sulfate and chondroitin sulfate) chains which are attached at three sites (14). These chains bind to cellular factors like laminins and elastins which (respectively) regulate elastic fiber assembly and basement membrane structure and integrity (14). Domain II is made up of four low-density lipoprotein (LDL) receptor-like regions and one immunoglobulin (Ig) like repeat. These components bind to proteins like Fibrillin-1 and provide the cell with proper connective tissue microfibril organization (14).

Domain III is comprised of three laminin B regions, which break up a longer stretch of eleven laminin epidermal growth factor (EGF)-like repeats. All vertebrate animals share this splitting of the EGF-like repeats and homology of this domain ranges from 60 percent up to 90 percent (14). Proteins like WARP bind to the second Laminin EGF-like repeat and mediate the chondrocyte pericellular matrix (14). Of all the perlecan domains, Domain IV is the most homogenous, with twenty-one Ig repeats that bind to components like nidogen-1 and collagen IV which regulate basement membrane integrity. Lastly, Domain V contains three modules with homology to laminin G chains separated by two EGF-like regions. These components bind to

proteins like ECM1 and alpha-distroglycan and aid in epithelial cell polarity and basement membrane organization (14).

MUTATIONS IN *HSPG2* DISRUPT SKELETAL DEVELOPMENT

Published works have linked mutations in *HSPG2* (most located in what would be Domains III and IV) to MCAs like Schwartz-Jampel Syndrome (SJS) and Dyssegmental Dysplasia Silverman-Handmaker Type (DDSH) (15–18). Overwhelmingly, mutations in *HSPG2* that lead to reduced levels of normal perlecan secretion into the extracellular matrix are associated with SJS while functional null mutations in which perlecan is not secreted into the extracellular matrix are exhibited in DDSH (1). SJS is a rare, autosomal recessive disorder characterized most notably by muscle stiffness (myotonia) and skeletal abnormalities (19). SJS Type 1A manifests early with predominately myotonia-related phenotypes while SJS Type 1B skews towards bone anomalies. SJS is also allelic to DDSH, a less frequent but more severe autosomal recessive disorder characterized by similar musculoskeletal deformities (19).

While skeletal abnormalities can differ in severity from patient to patient, patterns emerge wherein most patients diagnosed with SJS or DDSH have craniofacial abnormalities specifically, with conditions like micrognathia (a small jaw with a receding chin) (20) manifest in 30-79 percent of SJS patients and in 80-99 percent of DDSH patients (21,22). These manifestations of chondrodysplasia (disorders in the development of cartilage and later, bone) (23) suggest that mutations in *HSPG2* play a disruptive role in craniofacial bone development.

Previous studies looking at tissue staining showed that mutations in *HSPG2* cause abnormal chondrocyte proliferation and arrangement (15). Chondrocytes are differentiated cells found in cartilage, which later undergo the ossification process to become bone (24). Despite these publications, however, not much has been elucidated on the mechanisms that tie together

how mutations in *HSPG2* contribute to chondrocyte disorganization and how this phenomenon manifests as craniofacial abnormalities.

THE NEURAL CREST CELL LINEAGE AND BONE DEVELOPMENT

To understand the development of the craniofacial skeleton, there must first be a cohesive understanding of cellular development at the organism's earliest stages. Upon fertilization, the zygote undergoes cleavage and cell proliferation, the resulting cluster of cells is categorized as a blastula (25). This blastula must then undergo a process known as gastrulation, an evolutionary conserved set of movements which transform the single layer of the blastula into the multilayered structure of the gastrula (25).

In the first defining gastrulation movement, cells which will later form the deepest germ layer (the endoderm) and the middle germ layer (the mesoderm) undergo an epithelial to mesenchymal transition (EMT). These cells move below a more superficial layer of cells (the ectoderm) through an opening called the blastopore (in amniotic animals like humans, this is called the primitive streak) (26). After these cells have moved inward, epibolic movements evenly spread and thin the germ layers along the axis of the animal (26). In the third process, known as convergence and extension, these three layers of cells elongate on the anterior/posterior plane and narrow on the dorsal/ventral plane (26).

Following gastrulation, the embryo undergoes neurulation, otherwise known as the onset of developing nervous system. During neurulation, a portion of the ectoderm (described in the previous paragraph as the outermost germ layer) thickens into the neural plate and folds into the future neural tube (27). Upon closure, the neural tube will eventually give rise to the structures of the central nervous system. However, during neural tube closure, a subset of cells resident to the

dorsal end of the neural tube will delaminate and adopt a migratory phenotype (the epithelial to mesenchymal transition). These cells are known as neural crest cells (NCCs).

There are several derivative NCCs, which are classified into five distinct groups: trunk NCCs, vagal NCCs, cardiac NCCs, sacral NCCs, and cranial NCCs (28,29). Trunk NCCs give rise to neurons and glia that contribute to the periphery nervous system, vagal and sacral NCCs generate the enteric ganglia of the gut, cardiac NCCs participate in the development of the heart and cardiac ganglia, and cranial NCCs form craniofacial cartilage and bone (28,29). Of all four populations of NCCs, cranial NCCs (CNCCs) are the only ones that develop into cartilage and bone, making them vital to proper craniofacial skeletal development (30).

CNCCs migrate from hindbrain segments known as rhombomeres into the pharyngeal region (31). The stream of CNCCs starts as a solitary, uniform wave before splitting into three distinct, segregated streams, predominantly from rhombomeres 2, 4, and 6 (32). These three streams enter structures known as the pharyngeal arches, a grouping of six arches conserved across vertebrate species that are recognizable precursors for later craniofacial structures (32).

The first arch receives CNCCs from rhombomere 2 and develops maxillary and mandibular swellings which will give rise to the midface and mandible (lower jaw). The second arch receives CNCCs from rhombomere 4 and forms the stapes, the styloid process, and the lesser horns of the hyoid bone. The third arch receives CNCCs from rhombomere 6 and forms the hyoid body and the greater horns of the hyoid. The fourth and sixth arches (the fifth is not included as it only exists temporarily during embryogenesis) both contribute to the laryngeal cartilages (32).

Once these cells are situated in the pharyngeal arches, they begin to express transcriptional factors like *dlx2* and *dlx5,* a signal of their specification into the cranial lineage of

NCCs, which will eventually differentiate into chondrocytes (28). CNCC cells play a role in both intramembranous and endochondral ossification— a phenomena mediated by interactions with various mesodermal-derived cells in their immediate environment (33). In intramembranous ossification, CNCCs proliferate, condense into compact nodules, and become osteoblasts (committed bone precursor cells) (34). These cells directly lay the foundational base for bone growth. During the process of endochondral ossification, cells are first committed to become cartilage by expressing transcriptional factors thought to activate cartilage specific genes (*Pax1* and *Scleraxis)* (34–36). These committed cells then differentiate into chondrocytes (which express transcriptional factors like *col2a1*) and rapidly proliferate before becoming hypertrophic (37). Once these hypertrophic chondrocytes undergo apoptosis, osteoblasts begin forming bone matrix on the degraded cartilage and create bone (34,38). This complex procedure shows that NCCs are vital to craniofacial skeletal development and militainment.

ZEBRAFISH: A FUNCTIONAL MODEL FOR CRANIOFACIAL STUDIES

To understand the mechanisms underlying phenotypical abnormalities, researchers have historically used an assembly of animal models. Over time, the zebrafish has emerged as a complementary vertebrate model to the ubiquitous *mus musculus*, particularly in the developmental field (13,39). General advantageous reasons to use zebrafish include their high fecundity rate (about 200-300 embryos per clutch) and their external fertilization and transparency (which gives ease to genetic manipulation and imaging without incurring invasive procedures) (40). Additionally, craniofacial development employs the same embryologic processes and molecular pathways in most vertebrate animals, meaning that zebrafish studies can be translational to human development (41). This (coupled with their ease of use) makes them ideal models for the research described in this defense.

Complete sequencing of the zebrafish genome shows that they share 71 percent genetic homology with humans; 82 percent of human genes with morbidity descriptions are found in zebrafish as well (41). One such conserved gene is *hspg2,* the gene at the core of our research. Perlecan-null mice (mimicking the DDSH phenotype) typically die at embryonic day 10-12 due to mass hemorrhaging. This mass hemorrhaging is caused by increased mechanical stress (such as myocardial contraction) further weakening the basement membrane around the heart wall (42,43). This weakened connection between cardiomyocytes and surrounding endothelial cells allows blood to leak into the pericardial cavity and embryos die of heart arrest (43).

Unlike the murine model, zebrafish with *hspg2* knockdown does not cause hemorrhaging, perhaps circumventing the lethality by obtaining the majority of their oxygen intake via diffusion from their environment and not early cardiovascular function (13). There are currently alternative tissue specific manipulations of *hspg2* disruption, however these mice cannot be used to analyze *Hspg2* function during craniofacial development because they are created to express *hspg2* in chondrocytes to prevent lethal chondrodysplasia (44). Zebrafish likely circumvent this by having longer lasting maternal deposition (zebrafish embryos are transcriptionally active at 10 cell cycles) than mice (which are transcriptionally active as early as the 1-cell stage and robust in the 2-cell stage) (45–47). To lend credence to this, previous studies have shown that perlecan is present as early as the 64 and 1000-cell stages, both timepoints before embryonic transcription has begun (13).

In summation, the zebrafish model is ideal for studying how *hspg2* mediates craniofacial development. To explore the parameters of our patient case, we performed morpholino-mediated knockdown of *hspg2* in the zebrafish to examine resulting craniofacial phenotypes. Our initial hypothesis was that a knockdown of *hspg2* in the developing larvae would have a marked effect

on craniofacial development and structure. The following results (comprising of results drawn from WES, cell counts, qPCR, and *in situ* hybridization) support this hypothesis and suggest that *hspg2* regulates late stage NCC differentiation.

Chapter 2: Identifying mutations in the human *HSPG2* gene

METHODOLOGY

Subject DNA Extraction

The patient and parents were enrolled into a research protocol (COMRIB no. 07-0386) approved by the institutional review board at the University of Colorado School of Medicine. High quality, genomic DNA (A260/A280 ≥ 1.8 and A260/A230 ≥ 1.9) was extracted from whole blood obtained from the patient and parents using the Puregene Blood kit from Qiagen (Valencia, CA).

Whole Exome Sequencing and Data Analysis

Whole-exome sequencing was performed on the patient and his parents using service provided by Beijing Genomics Institute (Cambridge, MA). Details of data analysis were similar to procedure as previously described in Zhang *et al*, 2013 (48). Approximately 78 to 168 million, 100 bp, paired-end reads (>70X) were obtained and mapped to the reference human genome (GRCh37/hg19) using Burrows-Wheeler Aligner (BWA) (49). Variants were determined by the utilities in the SAMtools (49) and further annotated using SeattleSeq. Filtering and test of inheritance model were done using tools in Galaxy (50).

Variants were filtered against dbSNP build 137, 1000 Genomes (2010 version), Exome Variant Server (EVS, ESP6500SI-V2) and Exome Aggregation Consortium ExAC browser (version 0.3). Rare variants were identified when their minor allele frequency (MAF) was less than 1% using dbSNP137. The sequence data from the family was then used to test for causal variants under different inheritance models, including *de novo* mutation in a dominant model and compound heterozygous, homozygous and X-linked hemizygous mutations in recessive models. Candidate genes were further evaluated based on different criteria in each model. In the

dominant model, variants found in any database (dbSNP, 1000 Genomes, EVS, ExAC) were removed from the top candidacy list. In the recessive model, autosomal variants which had homozygotes found in the databases, such as EVS and ExAC, (or variants on chrX or chrY with hemizygotes in databases) were also removed from the top candidacy list.

Sanger Sequencing

Genomic DNA from the subject and parents (100 ng) was amplified using a set of primers (created in conjunction with Sigma (St. Louis, MO)) spanning *HSPG2*. The forward primer created had the sequence 5'-CCCAAGGACACACTTCCACT-3' and the reverse primer had the sequence 5'-AGGCAGGGAAGGAGCATAAT-3'. Promega (Madison, WI) GoTaq Green Master Mix and 10µM of each primer were used in the PCR master mix. The PCR began with an initial cycle at 95ºC for 5 minutes, followed by 35 cycles of 95ºC for 30 seconds, 61ºC for 30 seconds, and 72ºC for 1 minute, finishing with an extension at 72ºC for 5 minutes. The amplified PCR products were sequenced using the PCR primers as sequencing primers. The procedure was done on an Applied Biosystems Genetic Analyzer 3500 (Fisher, MA) with Applied Biosystems associated software at the Genomic Analysis Core Facility in The University of Texas at El Paso Border Biomedical Research Center.

RESULTS

Whole Exome Sequencing shows compound heterozygous mutations

Based on previous published information that stated that 15-25% of MCAs have some form of genetic etiology (4), it was hypothesized that the patient's phenotypical abnormalities were due to genetic mutations in the exome. Details of data analysis were previously described in the Methodology section. The paired-end reads done at >70X coverage (on average, each base was read by 70 sequences or more) were mapped to the reference human genome (GRCh37/hg19) using Burrows-Wheeler Aligner (BWA). Results are shown in Table 1.1. The coverage on the coding exon for the patient was 50.03, the mother was 93.38, and the father 63.10, respectively. The cutoff of this parameter lies at 50, meaning that the coverage (the number of reads mapped to the patient genome) was accurate for all three samples (ie: all three samples were evenly read and mapped) (51).

The variants were filtered against dbSNP137 (a database hosted by NCBI with a broad collection of single nucleotide polymorphisms) (52) and Exome Aggregation Consortium ExAC browser version 0.3 (dataset that aggregates data for allele frequencies that span 60,706 unrelated individuals) (53). The patient had variants spanning various genes: a heterozygous de novo mutation (a nonheritable mutation that has appears only in the patient) in the *CLIP4* gene, a homozygous mutation in the *SDK1* gene, and two compound heterozygous mutations (two mutations inherited from each parent in the same gene) in the *SPTAN1* gene and the *HSPG2* gene (Table 1.2).

Of these variants, only *HSPG2* has been linked to MCAs (SJS and DDSH) with craniofacial abnormalities as a hallmark phenotype.

Sanger Sequencing confirms compound heterozygous mutation in *HSPG2*

Results validated a c.5998-7A>G variant inherited from the mother in the noncoding promoter region and a c.4916C>T variant found in a EGF laminin domain inherited from the father (Figure 1.1). The father's mutation produces the amino acid Thr1639Met. Using multiple mutation prediction algorithms, it was predicted that this variant is deleterious (CADD: 29.1; PolyPhen2 = probably damaging (1); PROVEAN = deleterious (-3.37); SIFT = damaging (0.028); MutationTaster= disease causing (0.9999).

\

Table 1.1: Paired end reads show exome reading accuracy

A table showing the results derived from using the Burrows-Wheeler Aligner software. Listed are the patient and parents, the number of reads mapped to the coding and noncoding regions, the percentage in the coding region, and the overall coverage on the coding exon.

Patient ID	Reads Mapped to Coding Exon	Intergenic, Intronic, UTR%	Coding %	Coverage on Coding Exon (X)
Proband	23,645,253	46.84	53.06	50.03
Mother	43,943,738	54.18	45.82	93.38
Father	29,917,122	59.06	40.94	63.10

Table 1.2: Whole Exome Sequencing (WES) variants

A table showing the results obtained from WES. Listed are the positions of the mutations, the type of mutations, the name of the gene they were found in, the minor allele frequency (MAF) derived from each database, and the number of homozygotes in the databases.

Position	Type	Name	MAF (dbSNP142)	MAF (ExAC)	Notes
de novo (chr2:29375616)	Heterozygous	*CLIP4*	0.00002	0.000016	No homozygote in database
Homozygous (chr7:4091283)	Homozygous	*SDK1*	0.00879	0.005395	17 homozygotes in database
Compound Heterozygous (chr9:131341997)	Heterozygous (maternal)	*SPTAN1*	0.00158	0.00266	No homozygote in database
Compound Heterozygous (chr9:131395079)	Heterozygous (paternal)	*SPTAN1*	0.0006	0.000099	No homozygote in database
Compound Heterozygous (chr1:22181483)	Heterozygous (maternal)	*HSPG2*	0.00419	0.011	11 homozygotes in database
Compound Heterozygous (chr1:22188289)	Heterozygous (paternal)	*HSPG2*	0.0008	0.001318	No homozygote in database

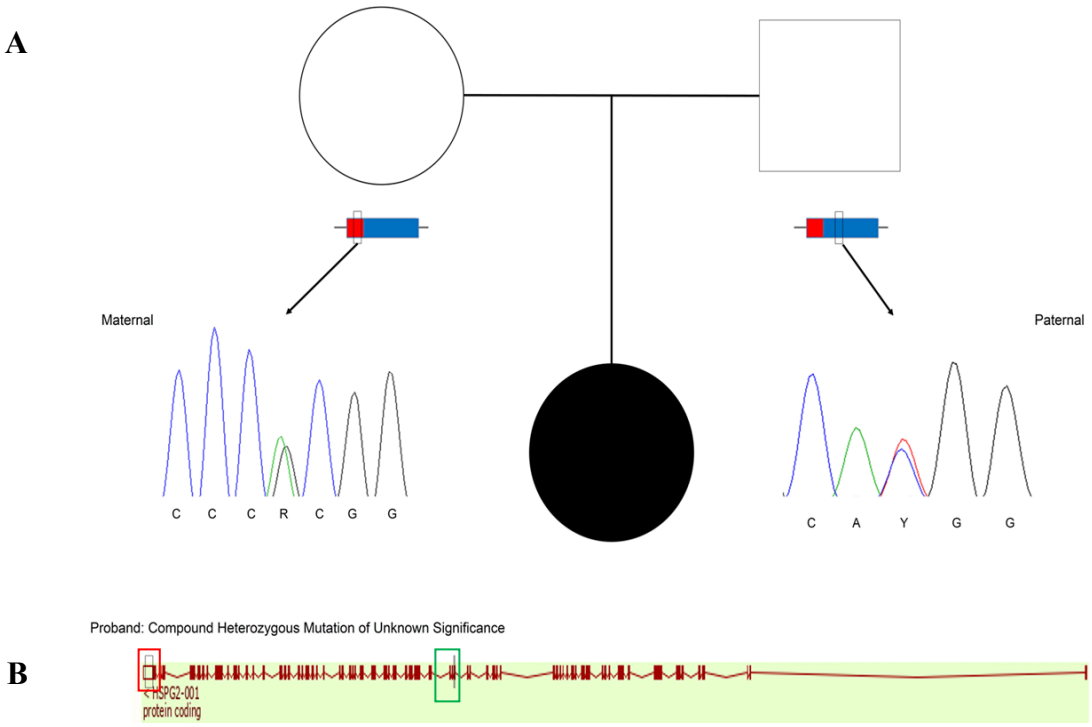

Figure 1.1: Sanger Sequencing confirms WES

A) A diagram showing the mutations inherited from both parents in conjunction with sequencing peaks (on the maternal end green and black overlapping peaks signify a base pair change from an adenine to a guanine and on the paternal end red and blue overlapping peaks signify a base pair change from a cytosine to a thymine). **B)** The intron-exon schema of the *HSPG2* gene. Region highlighted in red is where the maternal mutation is located relative to the sequence. Region highlighted in green is where the paternal mutation is located relative to the sequence.

Chapter 3: Antisense oligonucleotide morpholino knockdown of *hspg2*

PRELIMINARY RESULTS

Methodology

Animal Care

For all experiments, embryos were obtained by crossing adult Tg(*sox10*:tagRFP), Tg(*col2a1a*:EGFP), and AB wildtype fish. Embryos were maintained in E3 embryo medium at 28˚C. All zebrafish were maintained at The University of Texas El Paso according to the Institutional Animal Care and Use Committee (IACUC) guidelines protocol 811689-5.

Antisense oligonucleotide morpholino design and microinjection

Two antisense oligonucleotide morpholino sequences were designed in conjugation with Gene Tool LLC. The first was a translation blocking morpholino (MO) with the sequence 5'-TATCCTCGCCCCCATTTCTGCCAA-3', created to bind to the *hspg2* translation start site and sterically knockdown perlecan translation in the developing larvae. The second was a random control morpholino with the sequence 5'-AAAAAAAAAAAAAAAAAAAAAAAA-3', used to assure that the MO microinjections were not causing any form of cell death as described by previous literature (54). When injecting, the clutch of embryos were separated into three groups of equal numbers: the morphants (injected with the translation blocking MO), the random control group (injected with the random control MO), and the wildtype siblings (non-injected). Both MOs were injected into embryos at the one cell stage with a stock concentration of 0.10 µM and at a volume of 0.52 nL per embryo. All embryos were kept as described above until needed.

Alcian Blue Staining

On the first day of the procedure, zebrafish larvae (aged 5 days post fertilization) were fixed in 2% PFA in PBS, pH 7.5 for 1 hour at room temperature. Embryos were washed for 10

minutes with 100mM Tris pH 7.5/10mM MgCl2 before the Alcian blue stain pH 7.5: 0.4% Alcian blue (Anatech Ltd., MI) in 70% EtOH, Tris pH 7.5 (Fisher, MA), 1 M MgCl2 (Fisher, MA), EtOH (Fisher, MA), and H2O was added and left overnight at room temperature. On day two of the experiment, the embryos were destained and rehydrated using an EtOH: Tris pH 7.5 gradient. Embryos were bleached using a bleach solution: 30% H2O2 (Sigma, St. Louis, MO), 20% KOH (Fisher, MA) for 10 minutes. Samples were washed twice at 10 minutes per wash with 25% glycerol/0.1% KOH (Fisher, MA). Embryos were then stored at 4ºC in 50% glycerol/0.1% KOH (Fisher, MA) until measured. The distance between the Meckel's cartilage (an intermediate cartilaginous structure which makes up the ventral component of the mandibular arch) (55) and the ceratohyal (a pharyngeal arch cartilage which makes up the largest component of the ventral hyoid arch) (56) was measured for each embryo.

Transgenic animal lines and confocal microscopy

18 somite stage: Adult *Tg(sox10*: tagRFP) zebrafish were crossed and offspring were split into two groups: one group was injected with the translation-blocking morpholino and another was left uninjected as a wildtype control. Larvae were injected at the volume and concentration as described above. Petri dishes with developing larvae were left at room temperature overnight and monitored the following day. Larvae were fixed using 4% paraformaldehyde at the 18-somite stage (aligning with early NCC specification and migration in zebrafish). Fixed larvae were embedded on a dorsal plane in glass-bottomed plates using low-melt agarose. Larvae were imaged at 20X magnification using a Zeiss LSM 700 Confocal microscope with a 555 laser that exited the RFP reporter in *sox10* (a transcriptional factor expressed in NCCs) positive cells (39) . Maximum intensity projection images were processed and saved.

Prim-5 (1 dpf) stage: Adult *Tg*(*sox10*: tagRFP) zebrafish were crossed and offspring were split into two groups: one group was injected with the translation-blocking morpholino and another was left uninjected as a wildtype control. Larvae were injected as described above. Petri dishes with developing larvae were left at 28 °C and monitored the following day. Larvae were fixed using 4% paraformaldehyde at the Prim-5 stage (corresponding with NCCs migrating into the pharyngeal arches at around 1 dpf). Larvae all had approximately 30 total somites. Fixed larvae were embedded on a lateral plane in glass-bottomed plates using low-melt agarose. Larvae were imaged at 20X magnification using a Zeiss LSM 700 Confocal microscope with a 555 laser which exited the RFP reporter in *sox10* (a transcriptional factor expressed in NCCs) positive cells (39). Maximum intensity projection images were processed and saved.

Whole mount in situ hybridization and quantitative real time PCR

***In situ* hybridization:** Whole mount *in situ* hybridization was performed as described by Thisse and Thisse (57). Larvae were harvested and dechorionated at the Prim-5 (1 dpf) stage and fixed in 4% paraformaldehyde (Electron Microscopy Sciences, PA) overnight at 4ºC. Larvae were then dehydrated using a methanol: PBS gradient and stored in 100% methanol overnight at -20°C. Embryos were rehydrated using a PBS:Methanol gradient, washed in PBS with 0.1% Tween 20 and permeabilized with proteinase K (10ug/ml) for 10 minutes. Permeabilized larvae were prehybridized for 2 hours in hybridization buffer (HB) which consists as follows: 50% deionized formamide (Fisher, MA), 5X SSC (Fisher, MA), 0.1% Tween 20 (Fisher, MA), 50µg heparin (Sigma, MO), 500µg of RNase-free tRNA (Sigma, MO), 1M citric acid (Fisher, MA), and cell culture water. Larvae were then incubated overnight in fresh HB with an RNA probe (*dlx2a* at 127 ng) at 70°. On the second day of the procedure, samples were washed according to protocol, blocked in 2% sheep serum (Sigma, St. Louis, MO) and 2 mg ml-^{1} BSA (Sigma, St.

Louis, MO) for 2 hours at room temperature. Samples were then incubated with anti-DIG fragments (1:10,000) overnight at 4°C. On the third day, samples were developed with BM purple AP substrate (Sigma, St. Louis, MO) and imaged with a Zeiss Discovery Stereo Microscope fitted with Zen Software.

Quantitative PCR: For qPCR, RNA was isolated from embryos at 1 dpf with Trizol (Fisher, MA) according to manufacturer's protocol. Reverse transcription was performed using a Verso cDNA Synthesis Kit (Fisher, WA) and PCR was performed using an Applied Biosystems StepOne Plus machine with Applied Biosystems associated software. Sybr green (Fisher, MA) based primer pairs for each gene analyzed are as follows: *dlx2a* fwd CCTCACGCAAACACAGGTTA, *dlx2a* rev TGTTCATTCTCTGGCTGTGC, *rpl13a* fwd TCCCAGCTGCTCTCAAGATT, and *rpl13a* rev TTCTTGGAATAGCGCAGCTT. Statistical analysis of mRNA expression was performed using a student's two-tailed T-test, comparing the random control and *hspg2* morphant groups.

Results

Morpholino-induced knockdown of hspg2 causes craniofacial phenotypes

Previous studies performed in the murine model showed that deletion of *Hspg2* led to failure of the chondro-osseous junction of developing bones (15). In these studies (where 40 percent of the animals died at embryonic day 10.5), the lateral skeletal bones of the mutants were shorter, thicker, and misshapen when compared to wildtype mice. The remaining 60 percent of animals died shortly after birth and were characterized by a narrow thorax and craniofacial abnormalities. Based on these studies, we hypothesized that morpholino mediated knockdown of the zebrafish *hspg2* gene would cause craniofacial abnormalities as well. To test this, we performed Alcian blue stain to detect developing cartilage. Measurements on the Alcian blue stained embryos at 5 dpf (Figure 2.1) showed that the injection of the translation blocking morpholino caused a 7% truncation in the zebrafish mandible when compared to the random control and wildtype sibling groups. Stained embryos also demonstrated a fusion of the mandibular jaw joint between the Meckel's cartilage and palatoquadrate (the dorsal component of the mandibular arch) (58) in the morphants, a phenotype not present in either the wildtype or random control groups.

Neural crest cells migrate normally in the absence of hspg2

Because defects in the number of and migration of NCCs are possible mechanisms by which craniofacial deficits may arise (39), we hypothesized that the craniofacial abnormalities present at 5 dpf may have been due to *hspg2* affecting early NCC specification and migration. Images taken of *hspg2* morphants and wildtype siblings at both the 18 somite and Prim-5 stages (shown in Figure 2.2) showed no discernable differences between the sox*10* positive NCCs in either group at either timepoint.

hspg2 does not regulate dlx2a expression in cranial neural crest cells

One possible explanation for the phenotypes observed in morphants could stem from defects in CNCC specification. To determine if cells are specified into CNCCs properly, we performed whole mount *in situ* hybridization to measure the expression of *dlx2a* at 1-day post fertilization in random control and *hspg2* morpholino injected embryos. The expression of *dlx2a* (a homeobox gene) has been specified as a marker of proper CNCC specification at 1-day post fertilization in previous studies (59–61). *In situ* hybridization (Figure 2.2) revealed that there was no significant difference in the expression of *dlx2a* in morphants relative to random control injected embryos. Collectively, these data suggest that early CNCC development was normal and that the phenotypes we observed were likely caused by other mechanisms.

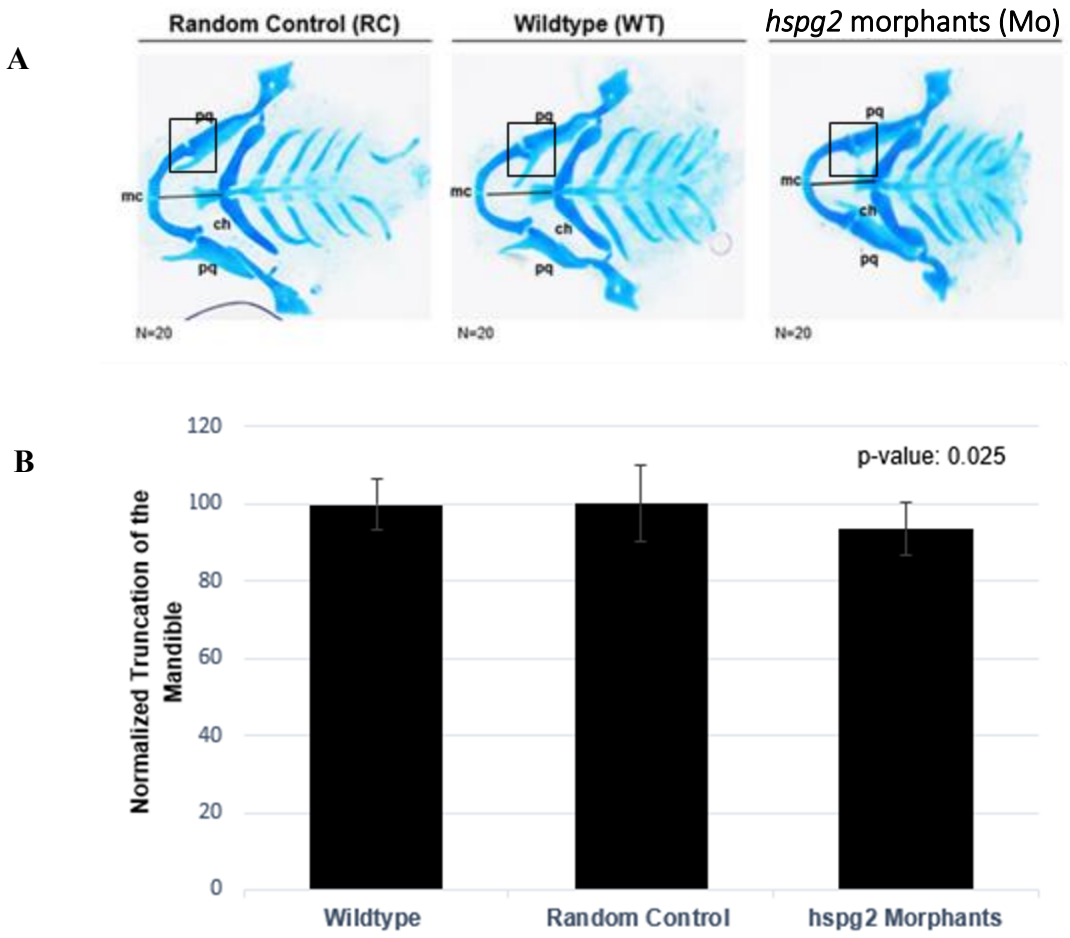

Figure 2.1: Alcian blue staining reveals craniofacial phenotypes

(A) Dissected representative samples for the wildtype, random control, and morphant groups. Ceratohyal, Meckel's cartilage, and the palatoquadrate are shown as the abbreviations (ch), (mc), and (pq) respectively. The black bar between the two shows the mandibular distance measured. The black box on each of the images shows the jaw joint. **(B)** The truncation of the mandible normalized to the random control group. The p-value shown pertains to the random control group and morphants.

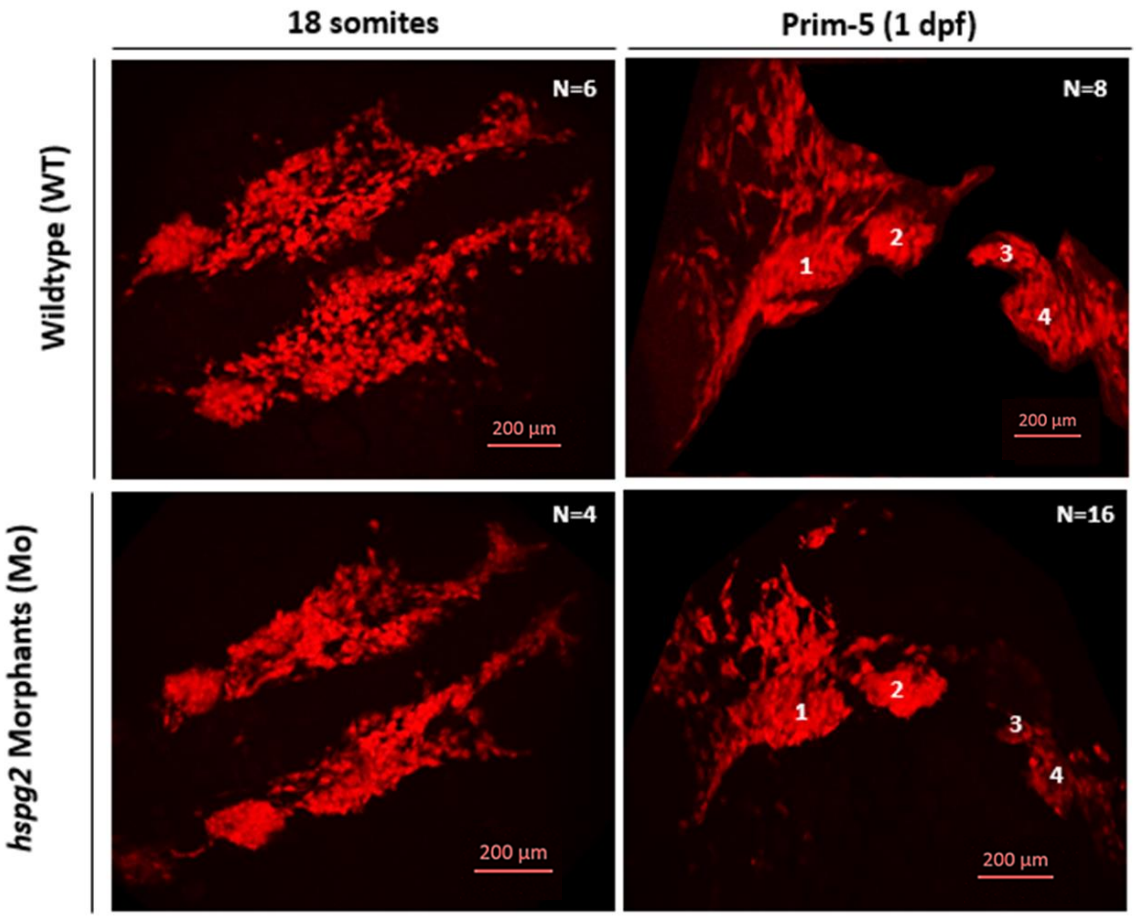

Figure 2.2*: hspg2* has no effect on early NCC migration or specification

Wildtype and morphant representatives at both the 18-somites stage and Prim-5 (~1 day post fertilization (dpf)) stage showing lateral streams of migrating NCCs (18 somites stage) and NCCs in the pharyngeal arches (labeled here 1-4) at the Prim-5 stage.

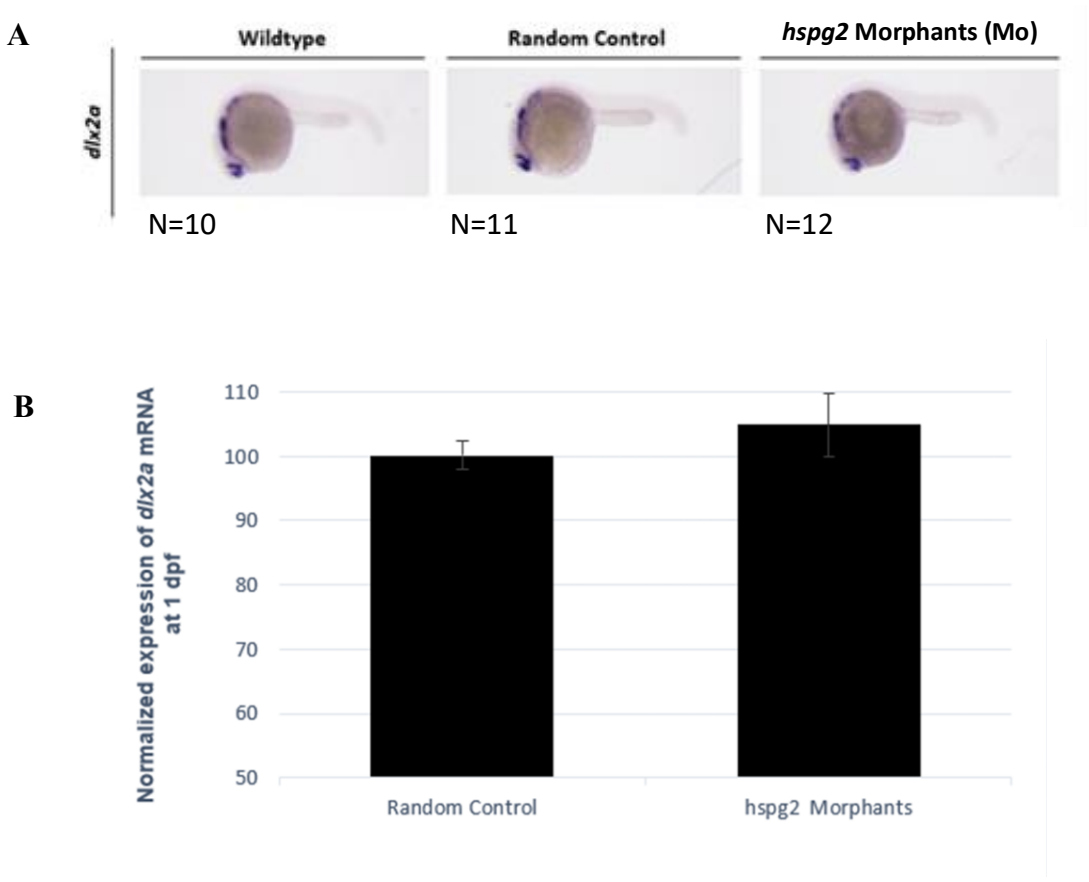

Figure 2.3: *hspg2* knockdown has no effect on *dlx2a* expression

(A) *in situ* hybridization of *dlx2a* groups at 1-day post fertilization (1 dpf). **(B)** Quantitative PCR expression of *dlx2a* in the random control and morphant groups at 1 dpf where each group has an N=15.

CURRENT RESULTS

Methodology

Alcian blue cell counts

The Alcian blue staining procedure was replicated at 5 dpf in the same manner as described in the methodology section above. A representative sample of each group (*hspg2* morphants, random control, and wildtype) was dissected and the viscerocranium (the mandibular jaw region) was mounted on a glass slide with 100% glycerol. A Leica microscope was used to take high-resolution color images of each sample and the chondrocytes at each jaw joint were counted (3 rows of chondrocytes on the left side of the joint and 5 rows of chondrocytes on the right). These numbers were selected because the left side of the developing jaw has a greater amalgamation of chondrocytes than the right.

Transgenic animal lines and cell counts

Protruding mouth stage (3 dpf): Adult *Tg*(*sox10*: tagRFP) zebrafish were crossed and offspring were split into three groups and injected as described above. Larvae were fixed using 4% paraformaldehyde at the protruding mouth stage (3 days post fertilization). All larvae were fixed according to ideal length (3.5 mm to 3.7 mm) as described on the Zfin Developmental Stages website (62). Larvae of each group were measured before and after fixation to assure all were within ideal size range and the same developmental stage. Total N= 10/group. Samples were then mounted on a ventral plane in glass-bottomed plates using low-melt agarose. Larvae were imaged at 40X oil using a Zeiss LSM 700 Confocal microscope with a 555 laser which exited the RFP reporter in *sox10* (a transcriptional factor expressed in NCCs) positive cells (35). 20 to 30 z-stack slices were obtained and the number of cells per z-stack at each jaw joint region

(3 rows of chondrocytes on the left side of the joint and 5 rows on the right) were counted using ImageJ.

Four-days post fertilization (4 dpf) stage: Adult *Tg*(*sox10*: tagRFP) and Tg(*col2a1a*:EGFP) zebrafish were incrossed and offspring were split into three groups and injected as described above. Larvae were injected as described above. Larvae were fixed using 4% paraformaldehyde at approximately 4 dpf. All larvae were fixed according to ideal length (3.7 mm to 3.9 mm) as described on the Zfin Developmental Stages website (62). Larvae of each group were measured before and after fixation to assure all were within size range and the same developmental stage. Representative samples (N=10) were then mounted on a ventral plane in glass-bottomed plates using low-melt agarose. Larvae were imaged at 40X Oil using a Zeiss LSM 700 Confocal microscope (the RFP larvae with the 555 laser and EGFP larvae with the 488 laser) which exited the RFP reporter in *sox10* (a transcriptional factor expressed in NCCs) positive cells and the GFP reporter in *col2a1a* (a transcriptional factor expressed in chondrocytes), respectively (35). 20 to 30 z-stack slices were obtained and the number of cells per z-stack at each jaw joint region (3 rows of chondrocytes on the left side of the joint and 5 rows on the right) were counted using ImageJ.

nkx3-2 mRNA quantification

***In situ* hybridization**: Whole mount in situ hybridization was performed as described by Thisse and Thisse (46). Larvae were harvested and dechorionated at the 2 dpf stage and fixed in 4% paraformaldehyde (Electron Microscopy Sciences, PA) overnight at 4ºC. Larvae were then dehydrated using a methanol: PBS gradient and stored in 100% methanol overnight at -20°C. Embryos were rehydrated using a PBS:Methanol gradient, washed in PBS with 0.1% Tween 20 and permeabilized with proteinase K (10ug/ml) for 10 minutes. Permeabilized larvae were

prehybridized for 2 hours in hybridization buffer (HB) which consists as follows: 50% deionized formamide (Fisher, MA), 5X SSC (Fisher, MA), 0.1% Tween 20 (Fisher, MA), 50µg heparin (Sigma, MO), 500µg of RNase-free tRNA (Sigma, MO), 1M citric acid (Fisher, MA), and cell culture water. Larvae were then incubated overnight in fresh HB with an RNA probe (dlx2a at 127 ng) at 70°. On the second day of the procedure, samples were washed according to protocol, blocked in 2% sheep serum (Sigma, St. Louis, MO) and 2 mg ml-1 BSA (Sigma, St. Louis, MO) for 2 hours at room temperature. Samples were then incubated with anti-DIG fragments (1:10,000) overnight at 4°C. On the third day, samples were developed with BM purple AP substrate (Sigma, St. Louis, MO) and imaged with a Zeiss Discovery Stereo Microscope fitted with Zen Software.

Quantitative PCR: For qPCR, RNA was isolated from embryos at 1 dpf with Trizol (Fisher, MA) according to manufacturer's protocol. Reverse transcription was performed using a Verso cDNA Synthesis Kit (Fisher, WA) and PCR was performed using an Applied Biosystems StepOne Plus machine with Applied Biosystems associated software. Sybr green (Fisher, MA) based primer pairs for each gene analyzed are as follows: *nkx3-2* fwd GCAGATTTAGCGGACGAGAC, *nkx3-2* rev GCTTCAACCACCAGCGTTAT , *rpl13a* fwd TCCCAGCTGCTCTCAAGATT, and *rpl13a* rev TTCTTGGAATAGCGCAGCTT. Statistical analysis of mRNA expression was performed using a student's two-tailed T-test, comparing the random control and *hspg2* morphant groups.

Results

Alcian blue staining reveals a loss of chondrocytes at jaw joint

Due to the morphants exhibiting a fusion in the mandibular jaw joint at 5 dpf, a deeper exploration of chondrocytes in the jaw joint at later developmental timepoints was needed. Based on the initial Alcian blue staining results, we hypothesized that we would find an abnormal arrangement of the chondrocytes in the mandibular jaw joint. Our replicated results (Figure 3.1) uncovered that morphants had fewer chondrocytes at both developing jaw joints when compared to the random control and wildtype groups. Despite the number of chondrocytes being decreased in the morphant jaw joint, the fusion was still present, suggesting that in addition to mediating cell differentiation, *hspg2* also likely mediates chondrocyte arrangement in developing cartilage.

hspg2 knockdown affects chondrocytes at jaw joint

Early studies performed in a murine model showed that *hspg2* knockdown decreased the number of chondrocytes in skeletal tissue (15). This literature in conjunction with results from earlier timepoints (18 somites and 1 dpf, discussed above in the preliminary data section), led us to hypothesize that if *hspg2* was not mediating early CNCC differentiation, that late stage differentiation could be disrupted. To test this, we performed analysis of *Sox10* positive cells at 3- and 4-days post fertilization. *Sox10* is a generalized marker of NCCs and at later time points is indicative of differentiation. At 3 dpf (Figure 3.2) morphants had a slight but statistically significant increase of *sox10:RFP* positive cells in the mandibular jaw joint region. However, by four days post fertilization, the number of *Sox10* positive cells was reduced relative to control injected embryos (Figure 3.3). Similar results were obtained when analyzing the number of *col2a1a* positive cells from the *Tg (col2a1a:EGFP)* larvae (Figure 3.3). Collectively, these data show a progressive loss of differentiated NCCs between 3 and 4 dpf.

hspg2 affects nkx3.2 expression

nkx3.2 (also called *bapx1)* was first identified in the drosophila model and is part of the NK family of homeobox genes (63). Homologues of the gene have been found in vertebrates (including zebrafish and humans) and are dorsally expressed in the first pharyngeal arch where the gene is essential for proper joint formation (63). Studies where the gene has been knocked down show a fusion of the jaw joint (63). We hypothesized that by measuring the expression of this gene on a transcriptional level, we could elucidate whether *hspg2* directly regulates joint development. *In situ* hybridization (Figure 3.4) demonstrate a decreased expression in the morphant groups when compared to the random control and wildtype groups. These results were quantified using qPCR (Figure 3.4).

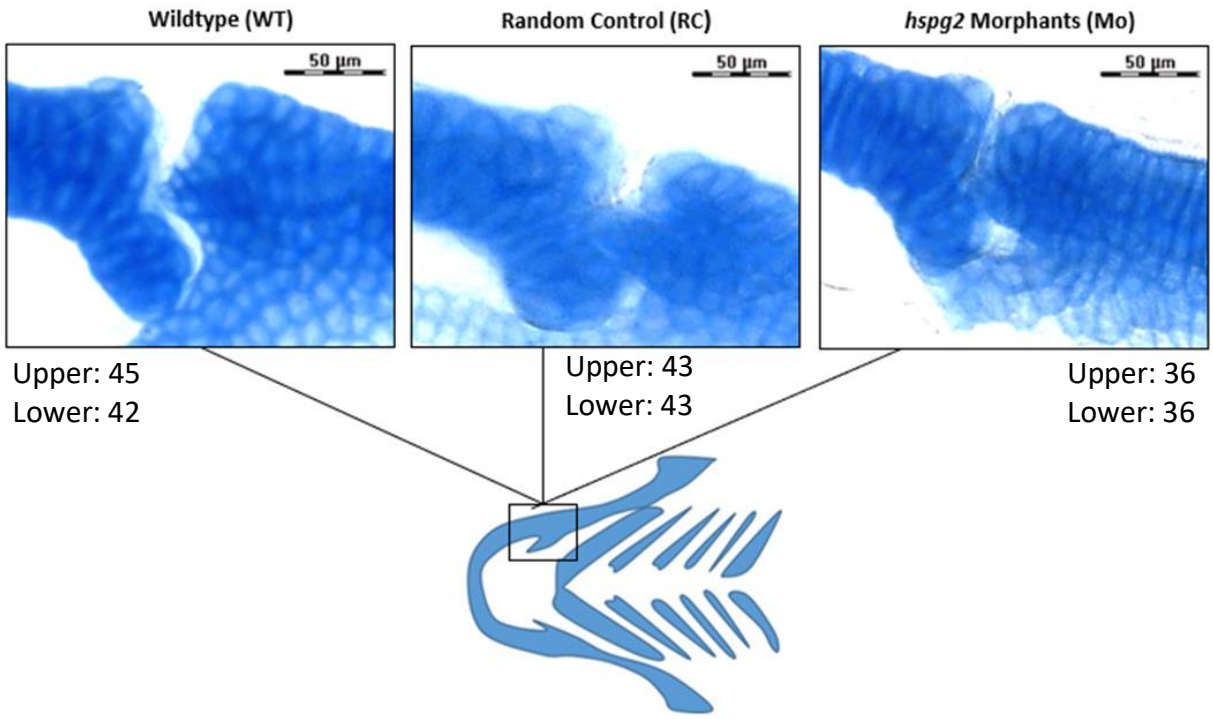

Figure 3.1: Alcian blue counts show a reduction of cells at the jaw joint

Representative samples of upper mandibular jaw joint in Alcian blue stained wildtype (WT), Random control (RC), and *hspg2* morphants (Mo) larvae. Number of chondrocytes counted (3 rows on the left side of the jaw and 5 rows on the right side of the jaw) in both joints shown below each representative depiction. Upper here stands for upper jaw joint and lower stands for lower jaw joint.

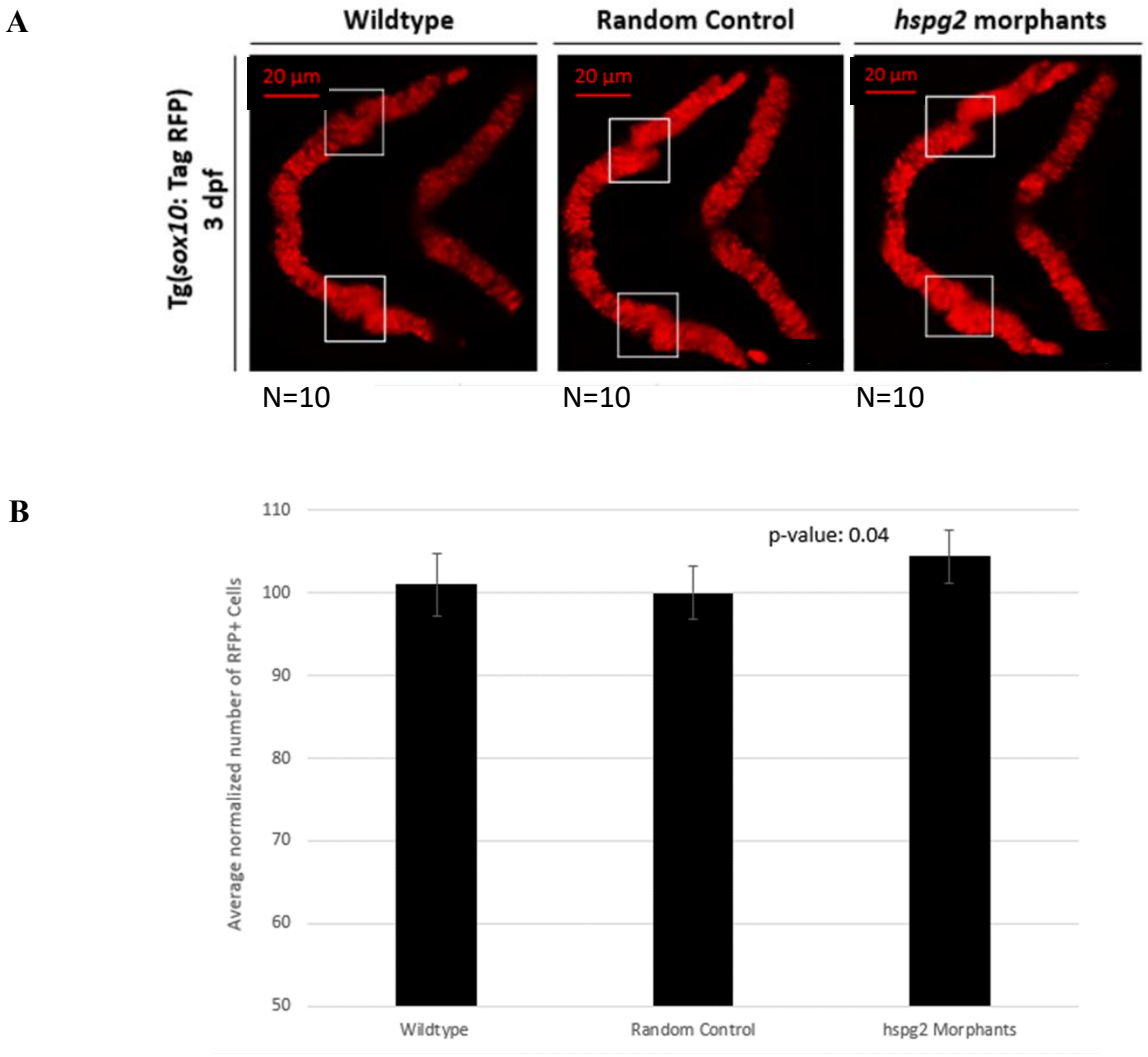

Figure 3.2: *hspg2* mediates RFP positive cells at 3 dpf

(A) A figure showing a representative sample of each of the three groups (Wildtype, Random control, and *hspg2* morphants) at 3 days-post fertilization (3 dpf). **(B)** A bar graph showing the normalized cell counts of RFP positive cells across all three groups. P-value pertains to the statistically significant difference between the random control group and the morphants.

A

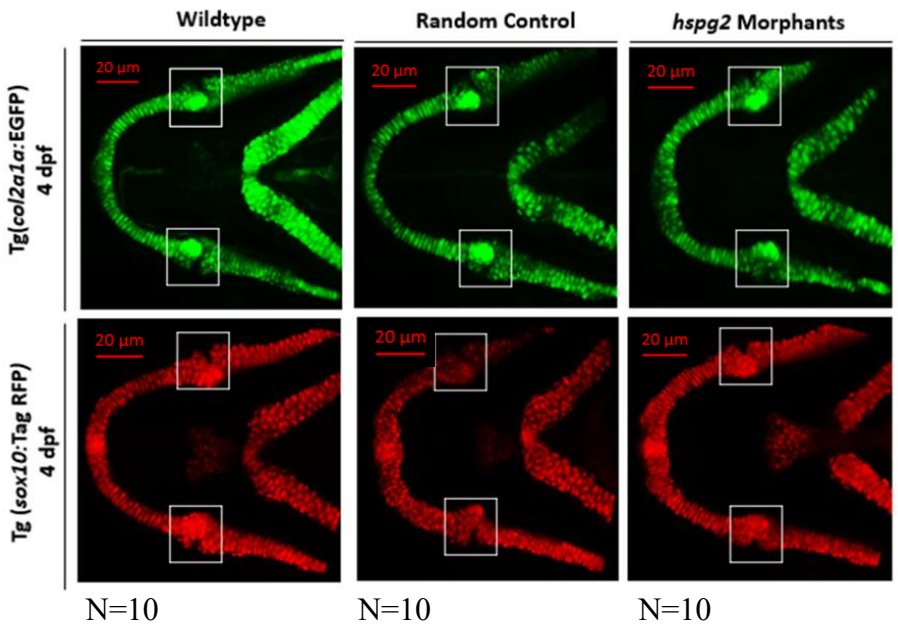
Wildtype
Random Control
hspg2 Morphants
Tg(col2a1a:EGFP) 4 dpf
Tg (sox10:Tag RFP) 4 dpf
20 µm
N=10
N=10
N=10

B

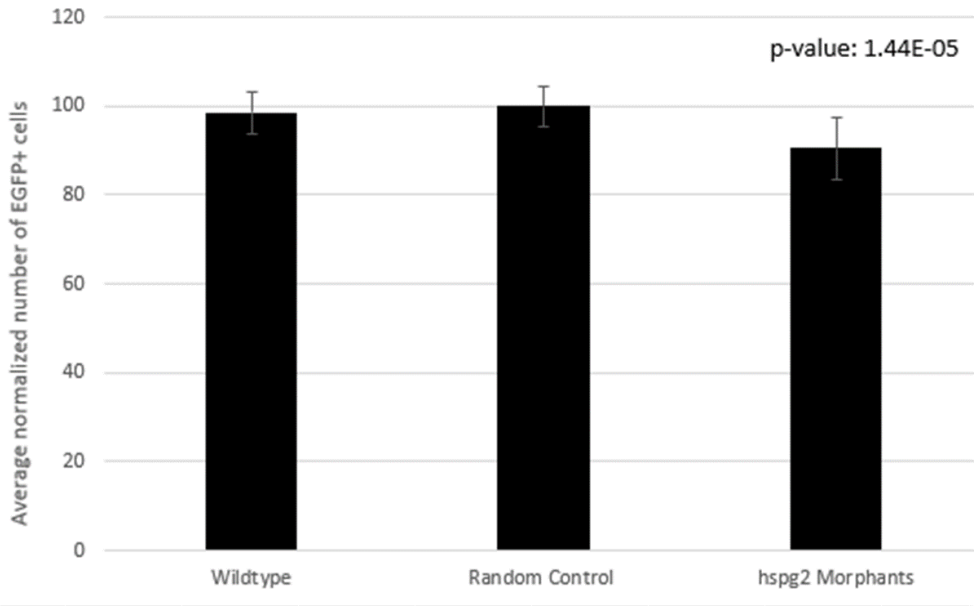
p-value: 1.44E-05
Average normalized number of EGFP+ cells
120
100
80
60
40
20
0
Wildtype
Random Control
hspg2 Morphants

C

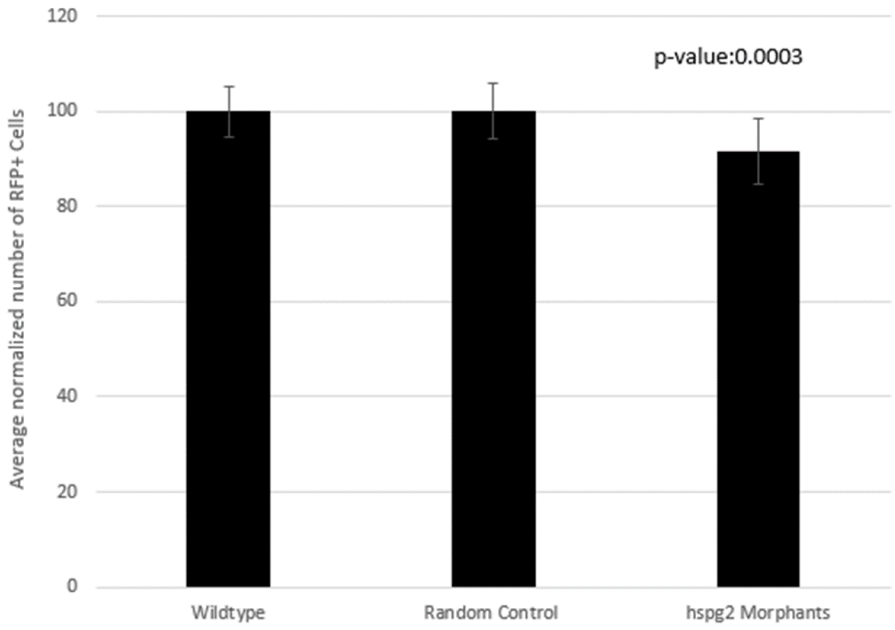

Figure 3.3*: hspg2* mediates chondrocyte numbers at 4 dpf

(A) Representative Wildtype, Random control, and *hspg2* morphant samples from transgenic *sox10:*RFP and *col2a1a*:EGFP lines. **(B)** Normalized cell counts of EGFP positive cells across Wildtype, Random control, and *hspg2* morphant groups. P-value pertains to the statistically significant difference between the Random control group and the morphants. **(C)** Normalized cell counts of RFP positive cells across Wildtype, Random control, and *hspg2* morphant groups. P-value pertains to the statistically significant difference between the Random control group and the morphants.

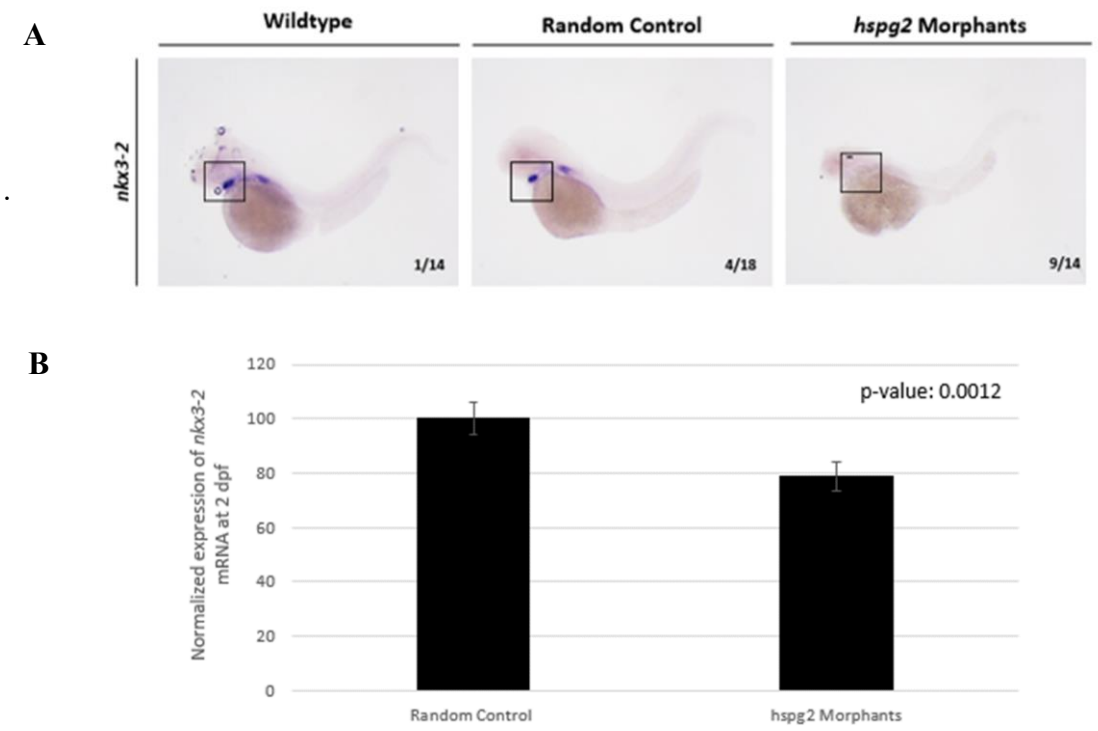

Figure 3.4: *nkx3.2* is decreased in *hspg2* morphants

(A) Representative *nkx3.2 in situ* figures of Wildtype, Random control, and *hspg2* morphant groups at 2 days-post fertilization**. (B)** Quantitative PCR expression of *nkx3.2* in the random control and morphant groups.

Chapter 4: *hspg2* CRISPR Cas 9 Mutant

CRISPR CAS 9 CREATION AND INJECTION

Introduction

In zebrafish, morpholinos have been shown to have off-target effects (64). To validate the morpholino experiments proposed, we used CRISPR/Cas9 to produce a stable, germline mutation in *hspg2*.

The acronym CRISPR stands for clustered regularly interspaced short palindromic repeats (65). These 29-nucleotide repeat sequences (separated by various 32-nucleotide spacer sequences originating in phages and adopted as a form of host immunity) were first reported in bacterial species. Partnering Cas enzymes were found to be highly conserved and adjacent to these repeat sequences (65). Later studies decoded the mechanism by which Cas9 and CRISPR RNA attack foreign DNA which matches that of the CRISPR sequences and found that this system could be manipulated.

The specificity of the CRISPR/Cas9 system depends on the structure and conformation of the Cas9 enzyme. This protein has two nucleic acid binding grooves: a large recognition (REC) lobe and a small nuclease (NUC) lobe which houses two domains (RuvC and HNH) and a protospacer-adjacent motif (PAM) interacting domain (65). When the enzyme is activated by a designed single guide (sg) RNA binding to the REC lobe, it uses Watson-Crick binding between the sgRNA and targeted DNA section to find a robust PAM site (NGG). Once the sgRNA is anchored at the proper PAM site, the HNH domain cleaves the sgRNA-DNA bond while the RuvC domain cleaves the other strand to form a double-strand break. These double strand breaks are repaired through non-homologous end joining (NHEJ). NHEJ employs DNA ligase IV to re-

join the broken ends, an operation that introduces insertion or deletion mutations (indels) into the DNA. This ability means that NHEJ has advantages in knocking out genes (65).

Methodology

Designing CRISPR Targets

DESKGEN cloud (a website which finds and scores CRISPR target sites across various genes) and PubMed nucleotide (a collection of genomic and transcript sequences from several sources including GenBank) was used to design a target site that spanned all *hspg2* variants at the earliest location. The target site selected has the sequence 5'-GGCGAGACGGTCACAGTAGG-3' and an activity score of 55 (where 35 is the cutoff for target accuracy). Sequence was found in the mRNA transcript and a pair of oligos (5'-TAGGCGAGACGGTCACAGTAGG-3' and 3'-AAACCCTACTGTGACCGTCTCG-5') covering the target site were found using ZiFiT Targeter Version 4.2 (a software package that identifies oligos for CRISPR target sites).

Creation of Plasmid for Cloning and Annealing Oligos

Plasmid Creation: A *pDR274* glycerol stock was used to grow plasmids on a Kanamycin resistant plate overnight at 37 °C. Two separate colonies were isolated overnight (18 hours) at 37 °C with shaking (225 RPM). Zymo plasmid miniprep kit (Irvine, CA) was used to extract bacterial DNA. Bacterial DNA was linearized (done to allow oligo insertion into the plasmid backbone) using Bsal-HF (New England Biolabs, MA) in a 37 °C water bath overnight. Cut plasmid purified using a DNA Clean and Concentration kit from Zymo (Irvine, CA), run on a 1% gel to assure enzyme functionality, and quantitated.

Annealing oligos: 3 µL of Oligos 1 and 2 (sequences listed above) were individually mixed with 5 µL10X T4 Ligase Buffer, 2 µL of PNK (Fisher, MA), and 40 µL of deionized water. Both

reactions were incubated at 37°C for 30 minutes and then annealed using the following parameters: 98 °C for 10 minutes, 70 °C for 20 minutes, and 37°C for 10 minutes. Annealed oligos were diluted 1:1000 using deionized water and ran on a gel with linearized plasmid. Oligos were quantitated and an online ligation calculator (66) was used to identify the amount of linearized plasmid and oligo concentrations needed for a proper ligation.

Cloning Target DNA

Ligation reaction was completed with the following measurements: 1 µL of 10X T4 Ligase Buffer (New England Biolabs, MA), 1 µL of T4 DNA Ligase (New England Biolabs, MA), 1 µL of linearized pDR274 vector DNA, 1µL of annealed oligos, and 5 µL of deionized water. Ligation mix was left overnight at 4°C. The following day, 8 µL of ligation mix was added to 50 µL of DH5α competent cells (New England Biolabs, MA) and mixed over ice for 30 minutes. Cells were heat shocked at 42°C for 20 seconds and then placed on ice for an additional 2 minutes. LB media was added and mixture was incubated at 37°C for 1 hour with shaking (225 RPM). 250 µL of transformed cell media was plated on Kanamycin-resistant plates and grown overnight (18 hours) at 37°C. 8 resulting colonies were screened for positive insertion. Positive colonies were sent for sequenced using an M13 fwd primer.

Creating sgRNA and Cas9 mRNA

Creating s*gRNA:* DNA from positive colonies was amplified via PCR and purified using the Zymo DNA Clean and Concentration Kit (Irvine, CA). Purified DNA was quantitated and synthesized into RNA using a T7 RNA polymerase kit from New England Biolabs (MA) in the following reaction mix: 100-500ng of purified PCR product, 2 µL of 10x T7 polymerase transcription buffer, 2 µl NTP mix, 1 µL RNase inhibitor, 2 µL T7 RNA polymerase, and 3 µL

of nuclease-free H2O. Reaction was left at 37° C overnight. Resulting RNA was purified using phenolchloroform and quantitated. 117.9 ng/µL aliquots were saved at -80°C.

Linearizing Cas9 mRNA: Glycerol stock sample of Cas9 (a protein related to the CRISPR mechaniscs) was grown and isolated as described above in plasmid creation section. Cas9 culture was isolated, extracted, and digested using the XBal enzyme from New England Biolabs (MA). Resulting RNA was purified using isopropanol washes.

Injection of Zebrafish Embryos

The following components were combined into a 10 µL reaction to inject into one-cell embryos: 4 µL of KCl (used here to aid embryo survival), 1 µL of Phenol red, 1 µL of 500 ng Cas9 mRNA, 1µL of 70 ng sgRNA, and 3 µL of deionized water. Embryos were injected as described in Chapter 3.

Methodology

DNA Isolation and PCR

Injected larvae were grown to adulthood. At approximately one year of age, DNA from each individual fish was extracted via fin clip and a series of phenolcholorform and ethanol washes. PCR primers that flank the genomic CRISPR target site were designed with the following sequences: *hspg2* fwd (5'-TTCGCACTGAATGAATCTGC-3') and *hspg2* rev (5'-GGGCACACCAATAGCAGAAC-3'). The PCR parameters were as follows: 95ºC for 5 minutes, followed by 35 cycles of 95ºC for 45 seconds, 60ºC for 30 seconds, and 72ºC for 30 seconds, finishing with an extension at 72ºC for 5 minutes.

T7 endonuclease digest

PCR was performed on DNA extracted from 24 injected fish using previously described *hspg2* primers. Additional DNA was extracted from 3 wildtype AB fish and 25 reactions were amplified using the same primer pair set. The reaction mix per tube was as follows: 5µL of a wildtype PCR reaction and 5 µL of potential CRISPR mutant PCR reaction (for samples 1-24), 10 µL of wildtype PCR reaction (negative control), and 5µL of *hcfc1a* PCR reaction and 5µL of wildtype PCR reaction (positive control). These samples were heated at 10 minutes for 95°C and then incubated at room temperature for 1 hour to reanneal DNA. After a 1-hour room temperature incubation, a cocktail of 1 µL of T7 Endonuclease enzyme, 2 µL of 10X buffer, and 7 µL of deionized water were added to each tube. Samples were analyzed for digestion on a 3% gel.

DNA ligation and sequencing

DNA from a potential screened mutant was ligated into DH5α component cells using a pGEM t-easy kit (Promega, WI). 8 colonies were selected and screened using the *hsgp2* primer pair described above. Positive samples were sent to sequence using the *hspg2* forward primer and fasta sequences were analyzed for possible mutations.

Wildtype outcross and the F1 generation

Potential founder mutant was outcrossed with a male wildtype fish in a 1 by 1 cross. DNA was extracted from 30 larvae at 2 dpf and amplified using the *hspg2* primer pair. Larvae DNA was screened using the T7 endonuclease assay in the same procedure as listed above. DNA of putative mutants was sequenced.

Results

T7 Endonuclease assay shows potential mutant

We utilized the T7E1 (T7 Endonuclease I) assay to screen for putative CRISPR-induced mutants. This assay is commonly used as an easy-to-interpret and cost-effective way of validating CRISPR-induced mutations (67). In bacteriophages, T7EI resolves branched DNA by cutting at the 5' base of cruciform DNA structures (67). When used in the T7E1 assay, the endonuclease will cut at sites where it recognizes a mismatched duplex structure. In this assay, both sample DNA and wildtype DNA are annealed to create a sequence that mimics a heterozygous mutation, which the enzyme will recognize and cleave. Samples 1-24 were compared to the wildtype negative control and an *hcfc1a* positive control with uncut samples having the same band size (285 bp) as the wildtype. Results (Figure 4.1) revealed seven possible mutants: Fishes 1, 3, 5, 7, 9, 11, 12, and 16. All seven PCR samples (about 5 μL each) were sent for sequencing along with the forward *hspg2* primer. Sanger sequencing results revealed that only fish 11 had a putative mutation within the amplified CRISPR target site.

Ligated colonies show two putative mutations within CRISPR target site

After Sanger sequencing results revealed a potential founder, we planned to confirm these data by ligating the putative founder's DNA into competent cells where changes in the target site sequence could be more readily analyzed. We hypothesized that we would detect a germline mutation from ligated bacterial colonies. Of the nine colonies screened, only seven contained the *hspg2* insert and these were each sequenced. Sequencing revealed distinct sequential changes in the CRISPR target site: a 4-bp deletion (CCTA) and a 2-bp insertion (CG) respectfully.

F1 generational outcross does not reveal a germline mutation

Because CRISPR injections tend to create mosaic mutations in different cell populations of the tested animal (and particularly so in zebrafish) (69), the only way to test if a putative mutation in the founder reached the germline would be to outcross the fish and test the potential F1 offspring. Results from the T7 digest showed five potential germline mutants. DNA from offspring were sent for Sanger sequencing and results did not show any abnormalities within the CRISPR target site, leading us to the conclusion that the initial discrepancies shown in the sequences from the colony ligations were mosaic mutations located in the caudal fin cell populations which did not achieve germline status.

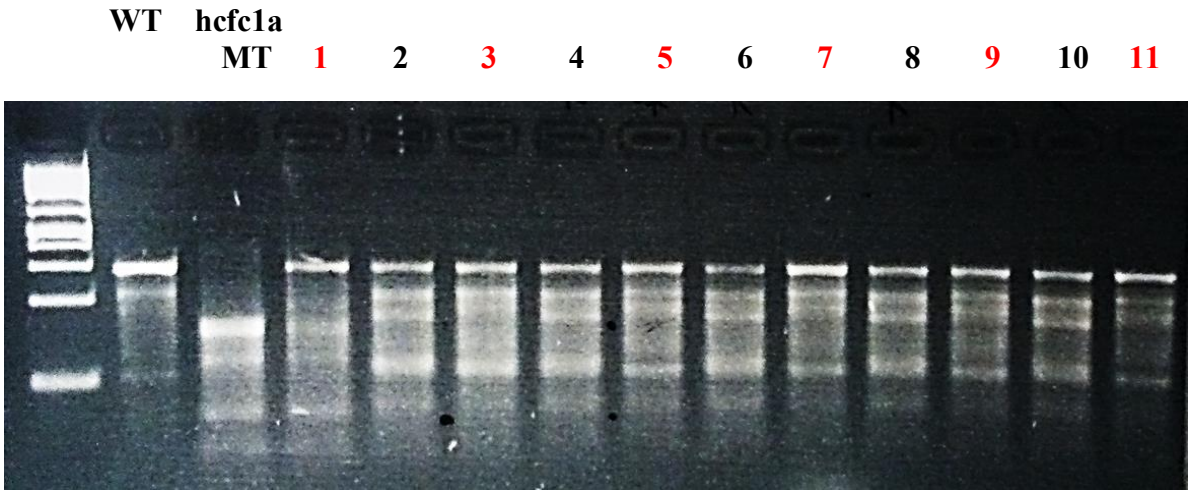

Figure 4.1: T7 digest reveals potential founder

Representative sample for 3% gel ran on T7 endonuclease assay. In figure, WT= wildtype and MT= mutant, with samples 1 through 11 representing the putative mutants tested. Numbers in red show the samples sent for sequencing. All samples selected differed from the wildtype (WT) by having two extraneous bands.

Chapter 5: Discussion

WES results for our patient case presenting with craniofacial abnormalities revealed an inherited compound heterozygous mutation in the *HSPG2* gene. Previous literature described craniofacial deficits as a hallmark phenotype of SJS and DDSH, two multiple congenital anomalies strongly linked to mutations in the *HSPG2* gene (21,22). Despite these parallels, very little is known about the mechanisms by which *HSPG2* regulates cartilaginous development. With the data described in this defense, we expand upon previously published work by identifying the complex role *hspg2* has regarding craniofacial development, particularly in the temporomandibular joint region.

Previous studies describing *Hspg2* knockouts in the murine model (15,18) confirmed that the *Hspg2* gene played a vital role in craniofacial development by reporting newly born *hspg2*$^{-/-}$ mice with truncated snouts and mandibles. Our initial Alcian blue stain results showed a similar phenotype, with a 7% mandibular truncation between the Meckel's cartilage and ceratohyal (analogous to the mandibular region) in the *hspg2* morphants. These results exemplify a correlation between our gene of interest and our resulting phenotype, which has been strongly supported by previous published literature (16–19,68–70).

Furthermore, we identified the presence of temporomandibular joint fusions in the morphant group. While patient cases have listed joint contractures in major joints as a common phenotype in SJS and DDSH patients (21,69–71), very little has been reported on this phenotype being present in the craniofacial region. In fact, in current published literature, there has been only one case report found that has shown that both craniofacial phenotypes (micrognathia) and limited range of motion in the jaw are present in patients with SJS (72). Although relatively novel, the idea of *hspg2* mediating the temporomandibular region is not completely unfounded.

Similar to all other diarthrodial joints in the human body, the temporomandibular joint contains a synovial capsule, which, in previous cell culture work, has been implicated to contain perlecan (73,74), the protein output of *hspg2*. Conclusively, although this jaw fusion in our morphants provides innovation to the field, it barely begins to introduce the role that *HSPG2* plays in mediating proper temporomandibular joint development and further studies would need to be completed to draw more concrete conclusions.

Previous studies (15,18) also revealed that knockout of *Hspg2* leads to abnormal chondrocyte arrangement and a loss of chondrocytes in hypertrophic zones of the appendicular skeleton. This lead us to the possible conclusion that mutations in *hspg2* could initiate temporomandibular abnormalities though the neural crest cell (NCC) lineage. Literature states that cells of the neural crest lineage must undergo a series of steps including specification, migration, proliferation, and differentiation in order to produce the cartilaginous structures of the face and neck (71,72). In this defense, we focused on the cranial neural crest cells (CNCCs) as these are the only NCC linage that lead to the formation of cartilage and bone in the craniofacial region (14). Nevertheless, a small concentration of morphants still presented with phenotypes like cardiac edema and pigmentation defects at 2 dpf, possibly suggesting a role for *hspg2* in various NCC lineages.

Results showing a decrease in *col2a1a*$^{+}$ (a transcription factor expressed in mature chondrocytes) cells at the temporomandibular joint at 4 dpf morphants implies that *hspg2* plays a mediating role in CNCC differentiation, something which is supported by *sox10*$^{+}$ counts at the same time point. Studies suggest that perlecan (*Hspg2*$^{-/-}$) deficient mice display an abnormal arrangement and proliferation of chondrocytes in the lateral skeleton (73). On a superficial level, these results match our obtained data, but gaps between the two still remain. The cells of the

appendicular skeleton derive from the mesoderm germ layer, not the ectoderm like the cells of the craniofacial skeleton (74). Although both lineages give rise to cartilaginous structures, the transcriptional factors that regulate skeletal development may play significantly different roles in the cells of each lineage. Additionally, the results we obtained from the *sox10*$^{+}$ cells in the same region at 3 dpf (an increased number in the morphants relative to the random control group) seem to directly counter the results at 4 dpf. To fully elucidate how *hspg2* is regulating the chondrocyte development in those regions, future studies would have to entail measurements of CNCC proliferation (through use of methods like 5-bromo-2′-deoxyuridine (BrdU pulse labeling) and CNCC apoptosis (through use of Terminal deoxynucleotidyl transferase dUTP nick end labeling (TUNEL) staining) (75,76).

As a departure from examining the cells of the CNCC lineage, we measured the expression of a transcription factor known as *nkx3.2. Nkx3.2* is a transcription factor expressed in pharyngeal arch one and it has been found in previous morpholino studies to align to proper temporomandibular joint development (63). We found that knockdown of *hspg2* causes chondrocyte dysregulation because chondrocytes filled the space of the developing joint, causing a fusion between the two bones. These results (in conjunction with the Alcian blue stain that revealed a temporomandibular fusion in the *hspg2* morphants) compelled us to use *nkx3.2* as a marker for jaw development.

Our results showed that a knockdown of *hspg2* reduced expression of *nkx3.2* as well. These results, when understood in the context of the decrease of *col2a1a*$^{+}$ cells found at 4 dpf, appear to match previous results done in mesenchymal cell culture which state that *nkx3-2* upregulates *col2a1* by directly binding to it (77). In this situation, diminishing the levels of *nkx3-2* appear to downregulate the expression of *col2a1a* and the differentiation of cells into

chondrocytes. Inversely, these results do not correlate to work done in the developing chick which states that *nkx3-2* is a negative regulator of chondrocyte maturation which, when knocked down, leads to an overproliferation of chondrocytes (78). Discrepancies in the results could be due to differences in the model used (although it is noted that the environment of the cell culture will not readily capitulate the dynamic environment that an *in vivo* model will) (79). Furthermore, these results which appear to match those that we received (the cell culture results) were performed in mesenchymal cells and not cells from an ectoderm lineage. To garner more consistent results, we would have to plan future studies where *sox10* and *col2a1a* are being measured quantitatively, perhaps with mRNA quantification taken at the 3 and 4 dpf stages.

An additional experimental technique would be to study the interaction between *hspg2* knockdown and *edn1,* a gene that encodes for a vasoconstrictor and is expressed in pharyngeal arch ectoderm, mesoderm, and endoderm (80,81). *Edn1* acts through its cognate type-A receptor (*Ednra*) to promote ventral skeletal fates and lower-jaw formation (81). *Edn1* has been reported to bind to *nkx3.2* and directly mediates its function (ie: expression of *edn1* is required for *nkx3-2* expression) (80).

As has been shown so far, the zebrafish is an ideal animal model to study the role of *hspg2* in craniofacial development. Induced knockouts (mimicking the null mutations associated with DDSH patients) in the murine model have resulted in embryonic lethality through mass hemorrhaging in the pericardial cavity, an occurrence which can be temporarily circumvented in the developing zebrafish (13). Subsequently, current mice models which survive to adulthood cannot be used to study skeletal development either because *hspg2* has been rescued in chondrocytes to prevent lethal chondrodysplasia (44).

In addition to the fish not requiring early mechanical heart function to obtain necessary oxygen intake (13), zebrafish generally make ideal models for lethal mutations due to their external fertilization and rapid development (82). Although cross-species staging comparisons are incredibly difficult to match, it can be implied that the murine embryonic day 10-12 time frame is analogous to the zebrafish pharyngula stages (1-2 dpf) through the larval protruding mouth stage (3 dpf) (83,84), both timepoints that have already undergone significant craniofacial development and can be easily monitored (62).

Nevertheless, all the work that has been reported using the zebrafish in this defense has been completed by use of a translation-blocking morpholino. While translation-blocking morpholinos are a simple and effective way in which to knockdown genes of choice, they tend to have off target effects and can be implicated in cell death via activation of p53 (54). In fact, it has also been reported that the phenotypes present in morphants very rarely match up with those present in a germline mutant (85).

We did, however, utilize a random control morpholino to account for the possibility of morpholino-induced cell death— an endeavor which proved to be rather successful (experiments performed did not show a discrepancy between the wildtype and random control groups). For future experiments, we plan on utilizing more than one morpholino control. A splice-site morpholino can aid us in mimicking the patient mutation more readily and a p53 morpholino can be co-injected to measure neural toxicity in a more accurate context (86).

Despite the use of morpholinos, the best manner in which you can test the true effect of genes implicated in disease is by creating a germline mutant. By creating a mutant, you can more readily rid yourself of off-target effects by breeding out the founder generation. Overall, our attempts of creating a CRISPR Cas9 mutant were unsuccessful and given the tendency for

CRISPR Cas9 to induce mutations at random, it is unlikely that we could have managed to create a germline mutation that replicated those found in the patient case. However, we predict future attempts will be successful to introduce nonsense mutations.

Conclusively, our results managed to create novel implications for the general association of *hspg2* in context of the development of the temporomandibular joint, a region of the craniofacial skeleton for which development has not been well elucidated. Our preliminary data concerning late CNCC differentiation raises pertinent questions about the fate of certain cells within different areas of the developing face. Further studies that elucidate the role of *hspg2* in skeletal development are warranted.

References

1. Martinez JR, Dhawan A, Farach-Carson MC. Modular Proteoglycan Perlecan/HSPG2: Mutations, Phenotypes, and Functions. Genes [Internet]. 2018 Nov 16 [cited 2019 Oct 26];9(11). Available from: https://www.ncbi.nlm.nih.gov/pmc/articles/PMC6266596/

2. Czeizel A. Definition of multiple congenital abnormalities. Acta Morphol Acad Sci Hung. 1981;29(2–3):251–8.

3. Common Multiple Congenital Anomaly Syndromes | Neonatology: Management, Procedures, On-Call Problems, Diseases, and Drugs, 7e | AccessPediatrics | McGraw-Hill Medical [Internet]. [cited 2019 Sep 17]. Available from: https://accesspediatrics.mhmedical.com/content.aspx?bookid=1303&sectionid=79662868

4. Agrawal S. Genetic Causes of Congenital Malformation. In 2007.

5. Brown TL, Meloche TM. Exome sequencing a review of new strategies for rare genomic disease research. Genomics. 2016 Oct 1;108(3):109–14.

6. ACMG Board of Directors. Points to consider in the clinical application of genomic sequencing. Genet Med Off J Am Coll Med Genet. 2012 Aug;14(8):759–61.

7. Wallace SE, Bean LJ. Educational Materials — Genetic Testing: Current Approaches [Internet]. University of Washington, Seattle; 2018 [cited 2019 Oct 14]. Available from: https://www.ncbi.nlm.nih.gov/books/NBK279899/

8. Schwarze K, Buchanan J, Taylor JC, Wordsworth S. Are whole-exome and whole-genome sequencing approaches cost-effective? A systematic review of the literature. Genet Med Off J Am Coll Med Genet. 2018;20(10):1122–30.

9. Rengasamy Venugopalan S, Farrow EG, Lypka M. Whole-exome sequencing identified a variant in EFTUD2 gene in establishing a genetic diagnosis. Orthod Craniofac Res. 2017 Jun;20 Suppl 1:50–6.

10. Rangel-Sosa MM, Figuera-Villanueva LE, González-Ramos IA, Pérez-Páramo YX, Martínez-Jacobo LA, Arnaud-López L, et al. Exome sequencing reveals three homozygous missense variants in SNRPA in two sisters with syndromic intellectual disability. Clin Genet. 2018;93(6):1229–33.

11. Baschal EE, Wethey CI, Swindle K, Baschal RM, Gowan K, Tang NLS, et al. Exome sequencing identifies a rare HSPG2 variant associated with familial idiopathic scoliosis. G3 Bethesda Md. 2014 Dec 12;5(2):167–74.

12. Reference GH. HSPG2 gene [Internet]. Genetics Home Reference. [cited 2019 Oct 15]. Available from: https://ghr.nlm.nih.gov/gene/HSPG2

13. Zoeller JJ, McQuillan A, Whitelock J, Ho S-Y, Iozzo RV. A central function for perlecan in skeletal muscle and cardiovascular development. J Cell Biol. 2008 Apr 21;181(2):381–94.

14. Farach-Carson MC, Warren CR, Harrington DA, Carson DD. Border patrol: insights into the unique role of perlecan/heparan sulfate proteoglycan 2 at cell and tissue borders. Matrix Biol J Int Soc Matrix Biol. 2014 Feb;34:64–79.

15. Arikawa-Hirasawa E, Watanabe H, Takami H, Hassell JR, Yamada Y. Perlecan is essential for cartilage and cephalic development. Nat Genet. 1999 Nov;23(3):354–8.

16. Arikawa-Hirasawa E, Le AH, Nishino I, Nonaka I, Ho NC, Francomano CA, et al. Structural and functional mutations of the perlecan gene cause Schwartz-Jampel syndrome, with myotonic myopathy and chondrodysplasia. Am J Hum Genet. 2002 May;70(5):1368–75.

17. Nicole S, Davoine CS, Topaloglu H, Cattolico L, Barral D, Beighton P, et al. Perlecan, the major proteoglycan of basement membranes, is altered in patients with Schwartz-Jampel syndrome (chondrodystrophic myotonia). Nat Genet. 2000 Dec;26(4):480–3.

18. Rodgers KD, Sasaki T, Aszodi A, Jacenko O. Reduced perlecan in mice results in chondrodysplasia resembling Schwartz-Jampel syndrome. Hum Mol Genet. 2007 Mar 1;16(5):515–28.

19. Stum M, Davoine C-S, Vicart S, Guillot-Noël L, Topaloglu H, Carod-Artal FJ, et al. Spectrum of HSPG2 (Perlecan) mutations in patients with Schwartz-Jampel syndrome. Hum Mutat. 2006;27(11):1082–91.

20. Micrognathia | Children's Hospital of Philadelphia [Internet]. [cited 2019 Sep 23]. Available from: https://www.chop.edu/conditions-diseases/micrognathia

21. Schwartz Jampel syndrome | Genetic and Rare Diseases Information Center (GARD) – an NCATS Program [Internet]. [cited 2019 Sep 23]. Available from: https://rarediseases.info.nih.gov/diseases/250/schwartz-jampel-syndrome

22. Dyssegmental dysplasia Silverman-Handmaker type | Genetic and Rare Diseases Information Center (GARD) – an NCATS Program [Internet]. [cited 2019 Sep 30]. Available from: https://rarediseases.info.nih.gov/diseases/2026/dyssegmental-dysplasia-silverman-handmaker-type

23. Chondrodysplasia - an overview | ScienceDirect Topics [Internet]. [cited 2019 Oct 17]. Available from: https://www.sciencedirect.com/topics/medicine-and-dentistry/chondrodysplasia

24. Chondrocyte - an overview | ScienceDirect Topics [Internet]. [cited 2019 Sep 17]. Available from: https://www.sciencedirect.com/topics/biochemistry-genetics-and-molecular-biology/chondrocyte

25. Animal development - Preparatory events | Britannica.com [Internet]. [cited 2019 Sep 17]. Available from: https://www.britannica.com/science/animal-development/Preparatory-events

26. Solnica-Krezel L, Sepich DS. Gastrulation: making and shaping germ layers. Annu Rev Cell Dev Biol. 2012;28:687–717.

27. Gilbert SF. Formation of the Neural Tube. Dev Biol 6th Ed [Internet]. 2000 [cited 2019 Oct 17]; Available from: https://www.ncbi.nlm.nih.gov/books/NBK10080/

28. Signals and Switches in Mammalian Neural Crest Cell Differentiation [Internet]. [cited 2019 Oct 18]. Available from: https://www.ncbi.nlm.nih.gov/pmc/articles/PMC3552505/

29. Cordero DR, Brugmann S, Chu Y, Bajpai R, Jame M, Helms JA. Cranial neural crest cells on the move: their roles in craniofacial development. Am J Med Genet A. 2011 Feb;155A(2):270–9.

30. Zhang D, Ighaniyan S, Stathopoulos L, Rollo B, Landman K, Hutson J, et al. The neural crest: A versatile organ system. Birth Defects Res Part C Embryo Today Rev. 2014;102(3):275–98.

31. Chapter 7. Neural Crest Cells in Craniofacial Skeletal Development | Elsevier Enhanced Reader [Internet]. [cited 2019 Oct 17]. Available from: https://reader.elsevier.com/reader/sd/pii/B9780124017306000089?token=BC0A683837CFFCD046BD8BAA87F96B19A1700A736E1E558BB517848CF3AEFDEAFEDD8FE175179F37AE1EB4AAAA9873BF

32. Mishina Y, Snider TN. Neural crest cell signaling pathways critical to cranial bone development and pathology. Exp Cell Res. 2014 Jul 15;325(2):138–47.

33. Mori-Akiyama Y, Akiyama H, Rowitch DH, de Crombrugghe B. Sox9 is required for determination of the chondrogenic cell lineage in the cranial neural crest. Proc Natl Acad Sci U S A. 2003 Aug 5;100(16):9360–5.

34. Gilbert SF. Osteogenesis: The Development of Bones. Dev Biol 6th Ed [Internet]. 2000 [cited 2019 Oct 27]; Available from: https://www.ncbi.nlm.nih.gov/books/NBK10056/

35. Šošić D, Brand-Saberi B, Schmidt C, Christ B, Olson EN. Regulation of paraxis expression and somite formation by ectoderm- and neural tube-derived signals. Dev Biol. 1997 May 15;185(2):229–43.

36. Cserjesi P, Brown D, Ligon KL, Lyons GE, Copeland NG, Gilbert DJ, et al. Scleraxis: a basic helix-loop-helix protein that prefigures skeletal formation during mouse embryogenesis. Dev Camb Engl. 1995 Apr;121(4):1099–110.

37. Intramembranous Ossification - an overview | ScienceDirect Topics [Internet]. [cited 2019 Oct 18]. Available from: https://www.sciencedirect.com/topics/veterinary-science-and-veterinary-medicine/intramembranous-ossification

38. Hatori M, Klatte KJ, Teixeira CC, Shapiro IM. End labeling studies of fragmented DNA in the avian growth plate: evidence of apoptosis in terminally differentiated chondrocytes. J Bone Miner Res Off J Am Soc Bone Miner Res. 1995 Dec;10(12):1960–8.

39. Quintana AM, Hernandez JA, Gonzalez CG. Functional analysis of the zebrafish ortholog of HMGCS1 reveals independent functions for cholesterol and isoprenoids in craniofacial development. PloS One. 2017;12(7):e0180856.

40. Five reasons why zebrafish make excellent research models | NC3Rs [Internet]. [cited 2019 Sep 23]. Available from: https://www.nc3rs.org.uk/news/five-reasons-why-zebrafish-make-excellent-research-models

41. Using Zebrafish to Test the Genetic Basis of Human Craniofacial Diseases - R. Grecco Machado, B. Frank Eames, 2017 [Internet]. [cited 2019 Sep 23]. Available from: https://journals.sagepub.com/doi/full/10.1177/0022034517722776?url_ver=Z39.88-2003&rfr_id=ori:rid:crossref.org&rfr_dat=cr_pub%3dpubmed

42. Sasse P, Malan D, Fleischmann M, Roell W, Gustafsson E, Bostani T, et al. Perlecan is critical for heart stability. Cardiovasc Res. 2008 Dec 1;80(3):435–44.

43. Costell M, Gustafsson E, Aszódi A, Mörgelin M, Bloch W, Hunziker E, et al. Perlecan maintains the integrity of cartilage and some basement membranes. J Cell Biol. 1999 Nov 29;147(5):1109–22.

44. Perlecan, a heparan sulfate proteoglycan, regulates systemic metabolism with dynamic changes in adipose tissue and skeletal muscle | Scientific Reports [Internet]. [cited 2019 Sep 30]. Available from: https://www.nature.com/articles/s41598-018-25635-x#Sec9

45. Harvey SA, Sealy I, Kettleborough R, Fenyes F, White R, Stemple D, et al. Identification of the zebrafish maternal and paternal transcriptomes. Dev Camb Engl. 2013 Jul 1;140(13):2703–10.

46. Maternal control of early mouse development [Internet]. [cited 2019 Oct 27]. Available from: https://www.ncbi.nlm.nih.gov/pmc/articles/PMC2834456/

47. Wragg J, Müller F. Transcriptional Regulation During Zygotic Genome Activation in Zebrafish and Other Anamniote Embryos. Adv Genet. 2016;95:161–94.

48. Zhang J, Lin H, Balaji P, Feng W. Optimizing Burrows-Wheeler Transform-Based Sequence Alignment on Multicore Architectures. 2013.

49. Li H, Durbin R. Fast and accurate short read alignment with Burrows-Wheeler transform. Bioinforma Oxf Engl. 2009 Jul 15;25(14):1754–60.

50. Goecks J, Nekrutenko A, Taylor J, Galaxy Team. Galaxy: a comprehensive approach for supporting accessible, reproducible, and transparent computational research in the life sciences. Genome Biol. 2010;11(8):R86.

51. Wang Q, Shashikant CS, Jensen M, Altman NS, Girirajan S. Novel metrics to measure coverage in whole exome sequencing datasets reveal local and global non-uniformity. Sci Rep. 2017 Apr 13;7(1):1–11.

52. Kitts A, Sherry S. The Single Nucleotide Polymorphism Database (dbSNP) of Nucleotide Sequence Variation. In 2011.

53. ExAC Browser [Internet]. [cited 2019 Sep 23]. Available from: http://exac.broadinstitute.org/

54. Heasman J. Morpholino oligos: making sense of antisense? Dev Biol. 2002 Mar 15;243(2):209–14.

55. Meckel's Cartilage - an overview | ScienceDirect Topics [Internet]. [cited 2019 Sep 23]. Available from: https://www.sciencedirect.com/topics/veterinary-science-and-veterinary-medicine/meckels-cartilage

56. ZFIN Anatomy Ontology: ceratohyal cartilage [Internet]. [cited 2019 Sep 23]. Available from: https://zfin.org/ZFA:0001400

57. Thisse C, Thisse B. High-resolution in situ hybridization to whole-mount zebrafish embryos. Nat Protoc. 2008;3(1):59–69.

58. Palatoquadrate - an overview | ScienceDirect Topics [Internet]. [cited 2019 Oct 27]. Available from: https://www.sciencedirect.com/topics/agricultural-and-biological-sciences/palatoquadrate

59. Zebrafish Zic2a and Zic2b regulate neural crest and craniofacial development. - PubMed - NCBI [Internet]. [cited 2019 Oct 20]. Available from: https://www.ncbi.nlm.nih.gov/pubmed/23665173

60. LaMonica K, Ding H, Artinger KB. prdm1a functions upstream of itga5 in zebrafish craniofacial development. Genes N Y N 2000. 2015 Apr;53(3–4):270–7.

61. Distinct Functional and Temporal Requirements for Zebrafish Hdac1 during Neural Crest-Derived Craniofacial and Peripheral Neuron Development [Internet]. [cited 2019 Oct 20]. Available from: https://journals.plos.org/plosone/article?id=10.1371/journal.pone.0063218

62. ZFIN Zebrafish Developmental Stages [Internet]. [cited 2019 Oct 21]. Available from: https://zfin.org/zf_info/zfbook/stages/index.html

63. Lukas P, Olsson L. Bapx1 is required for jaw joint development in amphibians. Evol Dev. 2018;20(6):192–206.

64. Morpholino artifacts provide pitfalls and reveal a novel role for pro-apoptotic genes in hindbrain boundary development [Internet]. [cited 2019 Oct 28]. Available from: https://www.ncbi.nlm.nih.gov/pmc/articles/PMC3111810/

65. Song G, Jia M, Chen K, Kong X, Khattak B, Xie C, et al. CRISPR/Cas9: A powerful tool for crop genome editing. Crop J. 2016 Apr 1;4(2):75–82.

66. LIGATION CALCULATOR [Internet]. [cited 2019 Oct 28]. Available from: http://www.insilico.uni-duesseldorf.de/Lig_Input.html

67. Sentmanat MF, Peters ST, Florian CP, Connelly JP, Pruett-Miller SM. A Survey of Validation Strategies for CRISPR-Cas9 Editing. Sci Rep. 2018 Jan 17;8(1):1–8.

68. Dyssegmental dysplasia, Silverman-Handmaker type, is caused by functional null mutations of the perlecan gene | Nature Genetics [Internet]. [cited 2019 Sep 30]. Available from: https://www.nature.com/articles/ng0401_431

69. Gomes RR, Farach-Carson MC, Carson DD. Perlecan functions in chondrogenesis: insights from in vitro and in vivo models. Cells Tissues Organs. 2004;176(1–3):79–86.

70. Hassell J, Yamada Y, Arikawa-Hirasawa E. Role of perlecan in skeletal development and diseases. Glycoconj J. 2002 May 1;19(4):263–7.

71. Minoux M, Rijli FM. Molecular mechanisms of cranial neural crest cell migration and patterning in craniofacial development. Dev Camb Engl. 2010 Aug;137(16):2605–21.

72. Lefebvre V, Smits P. Transcriptional control of chondrocyte fate and differentiation. Birth Defects Res Part C Embryo Today Rev. 2005 Sep;75(3):200–12.

73. Lowe DA, Srinivasan PP, Kirn-Safran C. Chondrocyte Phenotype of Mice Expressing Reduced Levels of Perlecan/HSPG2, an Essential Component of Cartilage. FASEB J. 2012 Apr 1;26(1_supplement):971.6-971.6.

74. Development of the Appendicular Skeleton | Anatomy and Physiology I [Internet]. [cited 2019 Oct 29]. Available from: https://courses.lumenlearning.com/suny-ap1/chapter/development-of-the-appendicular-skeleton/

75. Salic A, Mitchison TJ. A chemical method for fast and sensitive detection of DNA synthesis in vivo. Proc Natl Acad Sci. 2008 Feb 19;105(7):2415–20.

76. Kyrylkova K, Kyryachenko S, Leid M, Kioussi C. Detection of apoptosis by TUNEL assay. Methods Mol Biol Clifton NJ. 2012;887:41–7.

77. Kawato Y, Hirao M, Ebina K, Shi K, Hashimoto J, Honjo Y, et al. Nkx3.2 promotes primary chondrogenic differentiation by upregulating Col2a1 transcription. PloS One. 2012;7(4):e34703.

78. Provot S, Kempf H, Murtaugh LC, Chung U, Kim D-W, Chyung J, et al. Nkx3.2/Bapx1 acts as a negative regulator of chondrocyte maturation. Dev Camb Engl. 2006 Feb;133(4):651–62.

79. From in vitro Experiments to in vivo and Clinical Studies; Pros and Cons. - PubMed - NCBI [Internet]. [cited 2019 Oct 29]. Available from: https://www.ncbi.nlm.nih.gov/pubmed/26778084

80. Miller CT, Yelon D, Stainier DYR, Kimmel CB. Two endothelin 1 effectors, hand2 and bapx1, pattern ventral pharyngeal cartilage and the jaw joint. Dev Camb Engl. 2003 Apr;130(7):1353–65.

81. Nair S, Li W, Cornell R, Schilling TF. Requirements for Endothelin type-A receptors and Endothelin-1 signaling in the facial ectoderm for the patterning of skeletogenic neural crest cells in zebrafish. Development. 2007 Jan 15;134(2):335–45.

82. Allen JP, Neely MN. Trolling for the ideal model host: zebrafish take the bait. Future Microbiol. 2010 Apr;5(4):563–9.

83. Haudry Y, Berube H, Letunic I, Weeber P-D, Gagneur J, Girardot C, et al. 4DXpress: a database for cross-species expression pattern comparisons. Nucleic Acids Res. 2008 Jan;36(Database issue):D847–53.

84. Mouse Stages - Embryology [Internet]. [cited 2019 Oct 29]. Available from: https://embryology.med.unsw.edu.au/embryology/index.php/Mouse_Stages#Theiler_Stage_10

85. Kok FO, Shin M, Ni C-W, Gupta A, Grosse AS, van Impel A, et al. Reverse Genetic Screening Reveals Poor Correlation between Morpholino-Induced and Mutant Phenotypes in Zebrafish. Dev Cell. 2015 Jan 12;32(1):97–108.

86. Bedell VM, Westcot SE, Ekker SC. Lessons from morpholino-based screening in zebrafish. Brief Funct Genomics. 2011 Jul;10(4):181–8.

Vita

Barbara Castellanos received her Bachelor of Science (BS) at the University of Texas at El Paso in 2017. She entered the graduate school in the Fall 2017 semester on the Master of Science (MS) in Biological Sciences track. Over her graduate school career, she attended school conferences and presented her research. She was accepted to present a poster at the Society for Developmental Biology (SDB) conference in 2018 and was awarded a travel award by the Biological Sciences office at UTEP to attend. In late 2019, she was invited to give a formal talk on her research at the 2019 Texas Zebrafish Conference in Houston, TX. She ended her graduate school career having taught a variety of labs and having collaborated on a published book chapter discussing neural crest cells.

Contact Information: bcastellanos09@gmail.com